

Abstract

Robot technology is one of the pillars of modern society. Advances in information, electronic, and mechanical fields enable us to build and program machines to perform tasks in very different contexts, such as industry, surgery, and space missions.

Specifically, in manufacturing, robots are mainly used to perform repetitive and unhealthy works like assembly, welding and material handling, thanks to their mechanical robustness and ability to repeatedly perform the same movements with high accuracy and precision.

While in the early day, robot systems were constrained in isolated and known environments. Over the past few decades, robots have been asked to solve tasks in dynamic and unknown/partially-known environments, where they must **coexist** and **cooperate** with humans, while solving different **dynamic** tasks [1] (e.g. pick a requested object, whose position is not known a priori).

In this scenario, the desired characteristics of such robotic systems are: **(a) Adaptability to new conditions**, i.e., the system must be able to easily adapt to dynamic changes in system and environmental conditions, performing “*intelligent*” behaviors to handle these new scenarios and solve the desired task; **(b) Adaptability to new tasks**, i.e., the system must be able to easily adapt to both new variations of a known task and completely new tasks by exploiting experience to infer actions and solve them;

These requirements, can be challenging to achieve with traditional robot programming techniques based on hand-written policies and control methods. These conventional techniques often require a meticulous analysis of process dynamics, the construction of an analytical model, and the derivation of a control law that meets specific design criteria. This design process is tedious and time-consuming, particularly when high-level perception systems (e.g., cameras, microphones, motion sensors) are used to infer the state of the environment (such as the unknown position of a desired object relative to the end-effector) and the intentions of the human operator.

In contrast, significant advancements have been made by leveraging *learning techniques*, where the control policy is learned from data. This data can be generated either by **agent experience** [2] or by **expert demonstration** [3]. In the case of agent experience, there is a trial-and-error procedure where the control policy generates actions executed by an agent, which interacts with the environment. The parameters are then tuned according to the effectiveness of the actions, based on their impact on the environment relative to the task to be solved. In the case of expert demonstration, the control policy parameters are directly tuned using a dataset containing examples of task execution. The goal is to replicate the tasks observed in the dataset.

Specifically this thesis is framed in the context of *Learning from Demonstration* (LfD), a learning approach based on expert demonstration. According to the requirements of adaptability the thesis focus on a specific aspect of LfD named *Multi-Task LfD*. In this case, the control policy is not trained to execute a single task (e.g., picking an object) with the goal of generalizing across different objects and initial conditions [4, 5]. Instead, it is trained to handle various variations of a specific task (e.g., picking an object from different possible locations) [6] or even entirely different tasks (e.g., a single control policy that solves both picking and placing tasks as well as assembly tasks) [7, 8]. The goal is to generalize not only with respect to the objects

being manipulated and the initial conditions but also with respect to the tasks themselves. This means that by leveraging the knowledge-sharing hypothesis, we can achieve a system capable of solving new variations.

In this scenario, the learning procedure is much more challenging because we need to include and define the **conditioning signal** (i.e., the signal that informs the policy about the task to execute, the object to manipulate, and the target placing location). Additionally, the environment can contain **multiple distractor objects** (e.g., objects that can potentially be manipulated but are not of interest for a given task variation).

Regarding the conditioning signal, there are at least two intuitive approaches. The first is through a natural language description of the task to be executed [9, 10, 7], and the second is through a video demonstration [6, 8]. In the former, the task is described using phrases that specify the task details, such as “Pick the red box and place it into the first bin”. Given in input the phrase, the system must be able to infer the intent of the task (i.e., the pick-place operation) and the object of interest (e.g., red-box for picking and first bin for placing), and correlate this information with the environment and robot state to effectively control the robot. In the latter, another agent (either a robot or a human operator) performs the task in a different environment configuration, records this execution, and provides the video as input to the control policy. The control policy must then infer the intent from the video (i.e., the task to be performed, the object to be manipulated, and the final state) and control the robot to complete the task according to the agent’s state, the environment’s state, and the commanded task. Inspired by how humans can learn to replicate tasks by simply observing their execution, the main goal of this thesis is to develop a system capable of replicating tasks shown in a video demonstration. This involves addressing challenges related to extracting task-relevant information from the video, such as identifying the

manipulated object and its final position.

Regarding the issue of distractor objects, these are generally items that are not considered in manipulation operations, which simplifies the problem significantly. However, in the context proposed in this thesis, the problem is further complicated by the fact that the semantic meaning of an object of interest or a distractor is defined at run-time by the command itself. This means that if the initial configuration consists of four objects (e.g., four boxes of different colors), a specific object may or may not be of interest based on the command given to the robot.

The main contribution of this thesis is addressing the issue of distractor objects. Specifically, it was observed that a significant problem with the methods proposed in the literature is that while the learned control policy can generate valid trajectories, allowing the robot to reach, pick, and place objects, it often manipulates the wrong object. To address this problem, two main considerations have been made:

(1) The architectures proposed in current literature predominantly consist of end-to-end architectures, which translate high-level inputs such as images into corresponding actions. Consequently, the model must acquire an implicit representation capable of encoding both the task objective and the current state of the environment, including the location of the target object; (2) The learning procedure optimizes a metric that is not directly linked to task success but rather aims to replicate actions similar to those of the expert, on average.

These two aspects can lead to a control policy that is not able to effectively guide the robot toward the target object. Indeed, it was observed that one of the critical points during trajectory execution is the first steps. Small errors in these initial steps can result in reaching and consequently picking the wrong object.

Based on these considerations, this thesis evaluates the possibility of developing a system that explicitly reasons about the objects of interest (e.g., target object and placing location). The control module is

then directly informed with low-level information, such as the position of the target object.

To perform this explicit reasoning, a *Conditioned Object Detector* (COD) has been developed. This module, given the video demonstration and the current agent observation as input, predicts the class-agnostic bounding box related to the target object and the final placing location. This low-level positional information is then provided to the control module, which predicts the actions to perform.

The learning procedure is then divided into two steps. The first step involves training the *Conditioned Object Detector* (COD) module, which focuses on explicitly solving cognitive tasks, such as detecting regions of interest represented by the object to be manipulated and its final location. The second step involves training the *Object Conditioned Control Policy* (OCCP), which focuses on solving the control problem using low-level positional information that can be easily mapped into the corresponding actions.

The final system has been tested in both **multi-variation single-task** scenarios and **multi-variation multi-task** scenarios. Specifically, the system was evaluated on four different tasks: Pick-Place, Nut-Assembly, Stack-Block, and Button-Press. Each task had different variations based on the manipulated object and the final state. While the tasks share common properties, they also have specific characteristics. For example, the Nut-Assembly task involves contact-rich, precise manipulation, whereas Pick-Place can be solved in a much rougher manner.

Overall, the proposed methods demonstrated very promising behaviors and a general improvement over baseline methods that do not include object-related reasoning. This shows that solving manipulation tasks with an object-oriented approach can be an effective paradigm for LfD problems. Additionally, this approach provides interpretable information to the end user, as the predicted bounding boxes can be interpreted as the locations where the robot will move.

In conclusion, this thesis addresses the problem of leveraging object priors in the context of Multi-Task Imitation Learning. The proposed methods have been tested in both simulated and real-world scenarios, demonstrating their effectiveness.

Contents

1	Introduction	3
1.1	Application context	3
1.2	Motivation and thesis overview	3
1.3	State of the art	3
1.3.1	Problem formulation	3
1.3.2	Source of demonstration	7
1.3.3	Learning from demonstration	11
1.3.3.1	Behavioral Cloning	13
1.3.3.2	Inverse Reinforcement Learning	62
1.3.3.3	Generative Adversarial Imitation Learning	67
1.3.3.4	Learning from Observation	74
1.3.4	Graph Neural Network for planning systems . .	87
2	Conditioned object detector	89
2.1	Problem formulation	89
2.2	Architecture	89
2.3	Experiments	89
2.3.1	Dataset	90
2.3.2	Results	90
2.3.2.1	Target object detector	90
2.3.2.2	Target object and final position detector	90

3 Object conditioned control policy	91
3.1 Problem formulation	91
3.2 Architecture	91
3.2.1 Single control module	92
3.2.2 Double control modules	92
3.3 Experimental results	92
3.3.1 Dataset	92
3.3.2 Results	92
3.3.2.1 Single control module	92
3.3.2.2 Double control modules	93
4 Graph Neural Network for heuristic estimation	95
5 Real world application	97
5.1 Experimental Setting	97
5.2 Dataset	97
5.3 Results	97
6 Conclusions	99
Bibliography	99

ToDo.

- ToDo -

2

Chapter 1

Introduction

1.1 Application context

1.2 Motivation and thesis overview

1.3 State of the art

The chapter reviews the state of the art (SoTA) on the LfD problem. Specifically, Section 1.3.1 will focus on the formalization of the LfD problem. Then, Section 1.3.3 will present various approaches and methodologies for solving the LfD problem. This will include a detailed taxonomy of the different approaches, highlighting their pros and cons, and concluding with considerations relevant to the goals of this thesis.

1.3.1 Problem formulation

In this section, the problem of Learning from Demonstration, also known as Imitation Learning (IL), will be formalized.

The core idea behind IL is to program a robot by allowing a human expert to demonstrate how to solve a specific task. This approach avoids methods that demand intricate, handcrafted rules dictating the actions of machines and the dynamics of their operating environments, which require significant time and coding expertise. To achieve this goal, a way to transfer knowledge from the expert to the robot is necessary. One possibility is to leverage *data-driven* methods that can extrapolate control rules from demonstrated trajectories [3].

In this context, we need to define two general actors: the **expert**, who demonstrates the desired behaviors, and the **learner**, whose goal is to learn and replicate the behaviors demonstrated by the expert [3, 11]. Both the expert behaviors and the learner behaviors are described in terms of **policy**, generally denoted as π^E and π^L respectively.

Since IL relies on expert demonstrations, these are collected in a dataset $\mathcal{D}^E = \{(\tau_i^E, c_i)\}_{i=1}^N$, where:

- τ_i^E is the i^{th} demonstrated trajectory, generated by the expert policy $\pi^E \sim \tau_i^E$. It can be described as:
 - A *state-action sequence*, i.e., $\tau_i = [s_0, a_0, \dots, s_T, a_T]$, when the ground truth action performed by the expert is available.
 - A *state-only sequence*, i.e., $\tau_i = [s_0, \dots, s_T]$, when the ground truth action is not available.
- c_i is the *context-vector*, containing task-related information such as the initial state of the system s_0 , the position of the target object, or a representation of the task to be executed (e.g., a natural language description of the task or video demonstrations).

The state s_t can be defined in various ways. RGB images have been used in different works, either from a third-person point of view [12], representing the robot and its workspace, or from a first-person point of view with the camera mounted on the robot [13] or the gripper [10].

Additionally, 3D point-clouds generated by RGB-D images can also be used [14]. This high-level state representation can be enriched with proprioceptive signals such as joint positions, velocities, and torques [4].

Regarding the policy, the predicted action, \hat{a}_t , can be generated into two distinct ways. In one case, it is described as a *deterministic function*, meaning that it directly determines the action as follows: $\hat{a}_t = \pi^L(s_t, c_i)$ [13]. In the other case, it takes on a probabilistic definition, where it represents a probability distribution from which to sample the desired action: $\hat{a}_t \sim \pi^L(s_t, c_i)$ [8].

According to the definitions given in [3, 15], the learner policy π^L can be defined with respect to different abstraction levels:

- *Symbolic Characterization*, the policy maps states, and context to a sequence of options, i.e., $\pi : s_t, c \rightarrow [o_1, \dots, o_T]$, where each option is a sequence of actions. With this representation, complex tasks can be decomposed into a sequence of simple movements. However, it is hard to achieve an accurate task segmentation and motion ordering;
- *Trajectory Characterization*, the policy maps context to trajectory, i.e., $\pi : c \rightarrow \tau$. Because it allows the initial state to be mapped to a complete sequence of actions, this representation can be used to obtain the options in the Symbolic Representation. However, they need as many dynamic features as possible, that can be difficult to obtain;
- *State-Action Characterization*, the policy maps states(-context) to actions, i.e., $\pi : s_t, c \rightarrow a_t$. This representation makes it possible to map the current state directly to the corresponding action. However, it is easy for errors to accumulate in long-term processes. The action a_t can also be defined in various ways, depending on the type of control implemented by

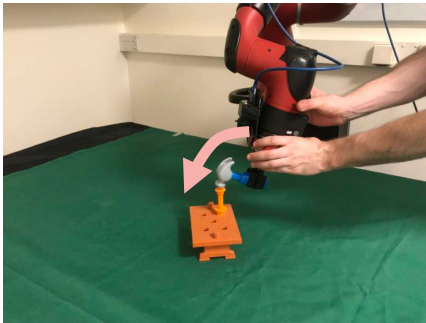
the method. Some methods operate in the joint-space, predicting motor control signals such as positions, velocities, and torques [4]. Other methods work in the operational space, where actions are assigned either an absolute pose with respect to a world frame \mathcal{W} , i.e., $a_i = [p_x^{\mathcal{W}}, p_y^{\mathcal{W}}, p_z^{\mathcal{W}}, r_x^{\mathcal{W}}, r_y^{\mathcal{W}}, r_z^{\mathcal{W}}]$ [8], or a displacement relative to the current gripper position, i.e., $a_i = [\Delta p_x^{\mathcal{W}}, \Delta p_y^{\mathcal{W}}, \Delta p_z^{\mathcal{W}}, \Delta r_x^{\mathcal{W}}, \Delta r_y^{\mathcal{W}}, \Delta r_z^{\mathcal{W}}]$ [13].

The expert and the learner, through their policies π^E and π^L , act on an environment modeled as a *Markov Decision Process* (MDP) [16]. An MDP is defined as a tuple (S, A, R, T, γ) , where:

- $S \subseteq \mathbb{R}^n$ is the set of states (e.g., joint positions and/or images).
- $A \subseteq \mathbb{R}^n$ is the set of actions (e.g., desired end-effector pose, desired joint torques).
- $R(s, a, s')$ is the *reward function*, which expresses the immediate reward for executing action a in state s and transitioning to state s' .
- $T(s'|s, a)$ is the *transition function*, which defines the probability of reaching state s' after executing action a in state s . This distribution, which describes the *system dynamics*, can be given a priori or learned (Model-Based methods), or it may not be considered at all (Model-Free methods).
- $\gamma \in [0, 1]$ is the discount factor, expressing the agent's preference for immediate rewards over future rewards.

With respect to the given MDP definition, the reward function plays different roles depending on the approach used:

- In *Behavioral Cloning* (BC) methods, the reward function is not explicitly used. Instead, a surrogate loss function is employed.



(a) Example of kinesthetic teaching [17]



(b) Example of teleoperation [4]

Figure 1.1: Examples of direct demonstration

- In *Inverse Reinforcement Learning* (IRL), the reward function is learned, under the assumption that the expert acts (near-)optimally with respect to some unknown reward function.
- In *Generative Adversarial Imitation Learning* (GAIL) and *Learning from Observations* (LfO), the role of the reward function varies based on the specific method, as will be explained in Section TODO.

1.3.2 Source of demonstration

As stated in Section 1.3.1, IL methods rely on a dataset \mathcal{D}^E of expert demonstrations. In this section, we will review the different ways to obtain these demonstrations, following the taxonomy proposed in [15].

Direct Demonstration

In the case of *Direct Demonstration*, the expert trajectory is a state-

action sequence, where the action is obtained directly from the robot. Specifically, the robot can be guided in task execution through *kineesthetic teaching* [18, 17], *teleoperation* [4, 19, 13, 7, 20, 21], or a (*hand-written policy*) [22, 6, 8, 23].

In kinesthetic teaching (Figure 1.1a), the human operator contacts and guides the robot, recording parameters such as the gripper pose, joint positions, and velocities. This has been one of the first approaches for the LfD problem [24, 25] because there is no need to consider differences in kinematics between human and robot. As a result, the data has less noise, and there is no need for expensive external tools for teleoperation. However, the robot must be passively controllable and require direct contact, which introduces safety problems and can be unintuitive for robots with multiple degrees of freedom.

In teleoperation (Figure 1.1b), the human operator remotely guides the robot with a joystick, control panel, or wearable device. These tools allow for higher safety since there is no direct contact between the robot and the human expert. Teleoperation systems have been used in various works. For example, the authors in [19, 26] proposed a teleoperation framework named Roboturk, which enables the collection of large-scale demonstration datasets [26, 5] for both simulated and real-world robots using a mobile phone as the controller. The authors in [4, 13, 7] used virtual reality controllers, allowing the human operator to intuitively move in the 3D environment, mapping the pose of the controllers to the corresponding gripper pose. This technology is of interest because it provides a safe and intuitive way to teleoperate a robot. However, the main drawback is the lack of haptic feedback, which can be mitigated by using haptic interfaces such as [27, 28].

Demonstrations collected with hand-written policies rely on the fact that the expert has access to ground truth information, such as the position of the object of interest. This assumption can be valid when a simulated environment is used to train, test, and validate the proposed methods, as seen in [6, 8, 23]. In these cases, the authors

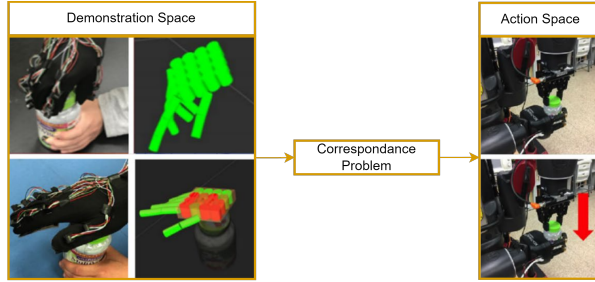
used a well-known simulation environment in the robotic learning community named Robosuite [29]. Here, demonstrations were collected to train methods using hand-written policies that have access to ground truth positional information about the object of interest, solving tasks such as Pick-Place, Nut-Assembly, Stack-Block, and more. Simulation environments facilitate the evaluation of the proposed methods and ensure reproducibility and consistent testing. The idea of using hand-engineered policies is not limited to simulation environments. Indeed, the authors in [22] used automatic grasping primitives combined with diagonal Gaussian distributions to collect demonstrations on a real-world robot. This approach aims to collect as many trajectories as possible with minimal human effort.

Indirect Demonstration

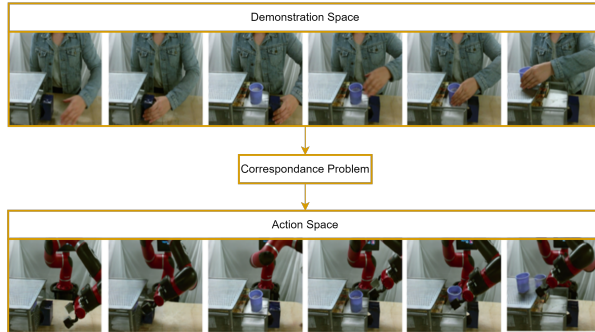
As discussed previously, in direct demonstration, an expert controls the learner agent and records the actions performed. The concept behind Indirect Demonstration (Figure 1.2) is to collect demonstrations that are completely disconnected from the target robotic platform. In the most promising scenario, a human demonstrator performs the desired tasks and records their operations. The learner, starting from this set of recordings, must be able to extrapolate the knowledge needed to replicate the observed tasks.

In this case, the expert demonstrations are state-only trajectories. Since the action space between the human demonstrator and the robot is different (consider just the different embodiment), it is not possible to directly use the human joint trajectories to minimize a supervised loss where the predicted value is related to the robot action space.

Initially, methods that follow this approach used wearable devices to capture human movement and record it [32, 30]. For example, in [32], the authors used a motion capture system to record the movement of a dancer and then transfer these trajectories to a humanoid robot.



(a) Example of indirect demonstration based on wearable device [30]



(b) Example of direct demonstration based on human video demonstration [31]

Figure 1.2: Examples of indirect demonstration

Similarly, in [30], the authors used a tactile glove [33] to record the movement performed by a human hand in the operation of opening bottles (Figure 1.2a).

In this line of research related to indirect demonstrations, there are also novel methods [31, 34, 35, 36, 37] that, inspired by the way humans learn by watching task execution, remove the assumption of having access to recorded human joint trajectories. In this case, the demonstrations are just videos of the human demonstrator (Figure

1.2b). Here, the system must infer from the video not only the intent of the task but also how this task can be solved and transform this information into its own action space.

Generally, methods based on wearable devices allow for very intuitive demonstrations, including critical information for manipulation tasks such as force and tactile information [30]. While methods based on just video demonstrations are very promising because they allow for the collection of demonstrations in the most intuitive and scalable way possible (potentially any video of a performed task can be used). However, both these approaches have to solve the *correspondence problem*, i.e., the system must be able to map motion captured in human space into the corresponding motion of the robot. In Section **TODO**, the different ways this problem has been solved in the context of visual demonstration will be explained in detail.

1.3.3 Learning from demonstration

This section is dedicated to presenting and analyzing various approaches for solving the LfD problem described in Section 1.3.1. Specifically, this section follows the taxonomy derived from studying different review papers [38, 39, 40, 15, 41, 11]. Figure 1.3 provides a graphical representation of the proposed taxonomy. The methods are first categorized based on the type of demonstration, either *State-Action* or *State-only*, followed by an overview of the different methodologies. The proposed taxonomy highlights the learning algorithm and main components for each methodology.

This chapter is divided into the following sections. Section 1.3.3.1 reviews methods for the fully-supervised learning methodology known as Behavioral Cloning.

Section 1.3.3.2 discusses methods under the umbrella of Inverse Reinforcement Learning, which solve the inverse optimization problem by first learning the reward function and then using it to guide policy

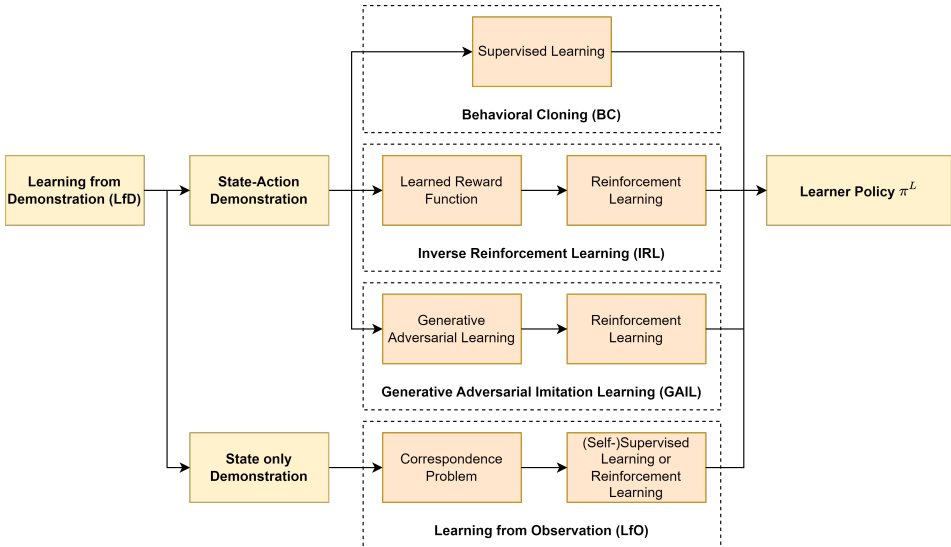


Figure 1.3: Taxonomy of LfD methods, divided based on type of demonstration and the learning algorithm used to learn the learner policy π^L

optimization following a reinforcement paradigm

Section 1.3.3.3 reviews methods leveraging the concept of *Generative Adversarial Learning* to optimize policy parameters and learn demonstrated behaviors, classified as Generative Adversarial Imitation Learning methods.

Finally, Section 1.3.3.4 covers the most recent methodology, Learning from Observation, characterized by optimizing the learner policy using state-only demonstrations. Each paragraph will present the research in the same way, i.e., the proposed works will be presented in a temporal order, highlighting the evolution of techniques and approaches over time. It is important to note that with respect to the problem managed in this thesis, the most relevant and most related literature

Algorithm 1 Abstract Algorithm for BC methods

Require: A set of expert demonstrations \mathcal{D}^E , a parameterized policy π_θ^L

Ensure: The optimal set of policy parameter θ^*

Optimize \mathcal{L} w.r.t. policy parameter θ using \mathcal{D}^E

is the one presented in Section 1.3.3.1. However, for sake of clarity and completeness, all the other approaches will be described with their pros/cons, with some considerations with respect to the proposal of this thesis. **ADD THIS DISCUSSION.**

1.3.3.1 Behavioral Cloning

Behavioral Cloning is one of the first approaches used to solve the LfD problem [42]. The high-level **supervised-learning** procedure followed by BC methods is outlined in Algorithm 1. Generally, BC methods take as input the expert demonstration dataset \mathcal{D}^E and a learner policy modeled as a parameterized function π_θ^L . The parameters θ can be either the weights of a neural network [42] or the parameters of a dynamic system [43]. As a supervised approach, the goal is to find the optimal parameters θ^* that can replicate the **ground-truth behaviors** contained in the dataset \mathcal{D}^E . This is achieved by solving an optimization problem, which can generally be described by Formula 1.1.

$$\theta^* = \underset{\theta}{\operatorname{argmin}} \mathbb{E}_{(\tau, c) \sim \mathcal{D}^E} [\mathcal{L}((\tau, c), \pi_\theta^L)] \quad (1.1)$$

In the following section, different ways in which the general optimization problem described by Formula 1.1 is formulated and solved will be discussed.

Dynamical Movement Primitives

The *Dynamical-Movement Primitives* (DMPs) methods are among the first successful applications of the BC methodology to the LfD problem. Their success is attributed to their ease of implementation and efficiency in learning. DMPs do not require learning or estimating the system dynamics, nor do they require a reward function or interaction with the environment during the learning procedure, as they are supervised learning methods.

DMPs were first formalized in [43]. They derive the policy directly in the trajectory space, allowing for explicit modeling of constraints such as smooth convergence toward the goal state. The core idea behind DMPs, as proposed in [43, 44], is to model the trajectory as a **point-to-point attractor system**, described by the set of differential equations in Formula 1.2.

$$\begin{aligned} \tau \dot{y} &= \beta_s(\alpha_s(g - s) - y) + f(z) \\ \tau \dot{s} &= y \\ \tau \dot{z} &= -\alpha_z z, \quad z(t) = z_0 \exp(-\frac{\alpha_z}{\tau} t) \end{aligned} \tag{1.2}$$

Here, β_s , α_s , and α_z are constants, s is the system state, z is the phase-variable function of time t , and f is the forcing term that describes the trajectory's non-linear behavior. Generally, f is a linear combination of basis functions $\psi_i(z)$ (e.g., Gaussian basis functions), such that $f(z(t)) = (g - s_0) \sum_{i=1}^M \psi_i(z(t)) \omega_i z$. Essentially, a DMP describes a point-attractor system where the current system state s must converge to the goal state g , starting from s_0 . In this context, the aim is to learn the set of weights $\{\omega_i, i = 1, \dots, M\}$, which can be obtained by solving a supervised learning problem with the loss

function described in Formula 1.3.

$$\mathcal{L}_{DMP} = \sum_{t=0}^T (f_{target}(t) - f(z(t)))^2 \quad (1.3)$$

The function $f_{target}(t)$ is equal to $f_{target}(t) = \tau^2 \ddot{s}_t^E - \beta_s(\alpha_s(g - s_t^E) - \tau \dot{s}_t^E)$ represents the evolution of the expert state s_t^E towards the goal state g , and represents the dynamic to mimic through the learned linear combination of basis function $f(z_t)$.

The initial DMPs formulation proposed in [43] has several issues that can be categorized as follows:

- **Handling stochasticity in demonstrations:** Different demonstrations can vary slightly due to differences in demonstrators, task completion methods, speeds, and paths. This variability creates a distribution in the demonstration space, requiring a method to manage it.
- **Defining different basis function:** In DMPs, the weights ω_i of the basis functions are learned. However, the force term can also be defined using other formalisms, such as Gaussian Mixture Models [45], Neural-Network Radial Basis Functions [46], or Gaussian Processes [47]. Therefore, the choice of how to model the force term is a hyper-parameter of the problem.
- **Managing arbitrary desired trajectories with intermediate via-points:** Once the behavior encoded in the demonstration is learned, generating novel trajectories that pass through new points (possibly defined by a human agent) is not possible. Therefore, a method to generalize to different waypoints is needed.
- **Handling high-dimensional inputs:** To use the DMPs algorithm, it is necessary to work in the robot space, recording

joint and gripper trajectories through teleoperation or kinesthetic teaching. However, in complex scenarios involving interaction with objects that do not have fixed initial positions, it becomes essential to infer the initial object state from high-level inputs, such as images.

To address these drawbacks, several solutions have been proposed. Notably, the authors in [48] introduced the *Probabilistic Movement Primitives* (ProMPs) framework. This probabilistic framework offers an alternative movement primitive representation, capturing the variability across different demonstrations and degrees of freedom (DoFs) through a covariance matrix. Specifically, the trajectory τ is modeled as a distribution: $\tau = \prod_t \mathcal{N}(s(t)|\Psi(z(t))^T \omega, \Sigma_s)$, where Ψ is a time-dependent basis matrix.

Generally, modeling the problem in probabilistic terms has several advantages, particularly the ability to generalize to new goals by conditioning the learned distribution on a given novel goal state [49].

To manage arbitrary desired trajectories, the authors in [50] proposed a novel framework for learning movement primitives, named *Via-points Movement Primitives* (VMP). VMP extends both Dynamic Movement Primitives (DMPs), which can only adapt to new start and goal positions but cannot directly handle intermediate via-points, and Probabilistic Movement Primitives (ProMPs), which can adapt to via-points within the statistical distribution of the demonstrated trajectories.

To achieve generalization across trajectories, the authors of VMP modeled the trajectory as a combination of two terms: the *elementary trajectory* h and a *shape modulation* f , expressed as $y(x) = h(x) + f(x)$ (Figure 1.4). The elementary trajectory serves as the foundational path that directly connects the start and goal of the demonstrated motion, and it can follow the formulation of a linear trajectory with constant velocity (Formula 1.4) or a minimum jerk trajectory (Formula

1.5). Specifically, the elementary trajectory can directly connect with linear segments two points that can be either the start and goal point, or the start and a via-point as well as the via-point and the goal point.

$$\begin{aligned} y(x) &= (y_0 - g)x + g + f(x) \\ h(x) &= (y_0 - g)x + g \end{aligned} \quad (1.4)$$

$$\begin{aligned} y(x) &= \sum_{k=0}^5 a_k x^k + f(x) \\ h(x_0) &= y_0 - f_0, \quad \dot{h}(x_0) = \dot{y}_0 - \dot{f}_0, \quad \ddot{h}(x_0) = \ddot{y}_0 - \ddot{f}_0 \\ h(x_1) &= y_1 - f_1, \quad \dot{h}(x_1) = \dot{y}_1 - \dot{f}_1, \quad \ddot{h}(x_1) = \ddot{y}_1 - \ddot{f}_1 \end{aligned} \quad (1.5)$$

In contrast, the shape modulation $f(x)$ is a linear model $f(x) = \psi(x)^T w + \epsilon_f$, where $\psi(x)$ is a Radial Basis Function and w is the set of learnable weights. This modulation term allows for adjustments to the trajectory to accommodate specific via-points.

In this framework, the learning procedure consists of two main components:

1. **Learning the shape modulation**, which involves learning the prior probability distribution of the parameter vectors w , characterized by the mean μ_w and variance Σ_w .
2. **Modifying the elementary trajectory**, which entails determining whether the requested via-point can be accommodated by adjusting the shape modulation or by introducing a new linear segment into the elementary trajectory.

To achieve this, VMP calculates the conditional probability of the shape modulation parameters given the desired via-point. If this probability exceeds a certain threshold η , the shape modulation is adjusted to ensure the trajectory passes through the via-point. However, if the probability is below η , indicating that the desired via-point is unlikely based on the learned prior probability of w , VMP will modify the elementary trajectory instead.

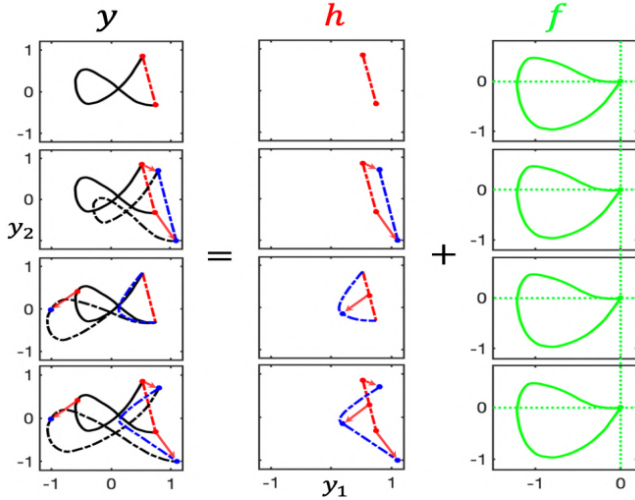


Figure 1.4: Graphical representation of the idea behind VMP [50]. The final trajectory y is represented as the sum of two components: the elementary trajectory h , and the shape modulation f . The elementary trajectory can directly connect two points (e.g., start and goal points) with a linear segment.

Overall, the VMP framework enhances the adaptability of movement primitives by enabling the robot to learn and adjust its trajectories based on a limited number of demonstrations and specified via-points, making it a practical solution for various robotic applications.

In addition to these methodological advancements, several works have leveraged DMPs to solve specific robot manipulation problems [51, 18, 52]. In all of these cited works, DMPs have been employed to address the problem of task decomposition, specifically the identification of different skills (e.g., pick, pour, place, reach, etc.) involved in a task.

For instance, in the preliminary work [51], the authors used a set of predefined motion primitives modeled as DMPs. The objective was to recognize these primitives within the demonstrated trajectory using an Expectation-Maximization algorithm. Similarly, in [18], DMPs were utilized to learn and reproduce motion primitives from demonstrations during the kinesthetic teaching of structured tasks. In this work, action segmentation was performed based on either object proximity or explicit human commands. When the robot manager identifies a new action, the corresponding DMP is learned, and the sequence of tasks is organized into a hierarchical structure.

Despite all the successfully applications saw previously, DMPs and all the variants have a very relevant limitation, that is related to the difficulty of handling high-dimensional input such as images. For this reason, the scientific community has focused the attention on methods that leverage deep architecture, that will be explained in detail in the following paragraphs.

Single-Task Imitation Learning

This paragraph will review the research conducted in the context of Single-Task Imitation Learning. Specifically, within the scope of robotic manipulation problems, the term “Single-Task” indicates that the learned policy π^L can perform only the specific task it has been trained on. For example, if the task involves a pick-and-place operation with a fixed place position, the model cannot handle variations in the place location. Additionally, the focus will be primarily on methods that use high-level state representations, such as images, processed by deep architectures to solve the problem.

In this scenario, the scientific literature extends far back in time. One of the seminal works in this field was proposed in 1988 by Pomerleau, who introduced *ALVINN* [42]. ALVINN is an autonomous vehicle driving system based on a Neural Network that predicts the

steering angle from a synthetic camera image input. The network was trained on pairs of (image, steering angle), with the training procedure framed as a supervised classification problem. This was achieved by discretizing the steering angle into 45 units. Pomerleau’s work immediately highlighted the issue of **compounding error**, which arises from the **covariate shift phenomenon**. This issue occurs because an action a_t influences the subsequent state s_{t+1} , which becomes the next sample, thereby violating the i.i.d. assumption of Supervised Learning. This results in a test-data distribution that may differ from the training one. This phenomenon has significant consequences on the expected performance of the system and is addressed by methods discussed in the section on *Interactive Imitation Learning*.

Despite the covariate-shift problem, [4] showed that very interesting performance can be obtained in the context of Robot Manipulation, by means of Behavioral Cloning and high quality demonstrations given by teleportation system. In this work, a Convolutional Neural Network was trained to predict the desired linear-velocity, angular-velocity of the end-effector, and the binary gripper state (open/close), given in input the current RGB-D observation of the scene, and the position of three points of the end-effector, during the last 5 time-steps (Figure 1.5). The system was tested on 10 tasks, and the performance are reported in Table 1.1. The proposed system achieved a high success rate while evaluating all the tasks. The tests were carried out from different initial conditions but still quite similar to those present in the training set (e.g., the initial object positions have been uniformly distributed within the training regime, with random local variations around these positions). The analysis of failure cases showed that the leading cause of errors was the inability to detect critical points in the task execution, such as closing/opening the gripper to pick/place the object or detect the position of the object of interest in order to avoid collision with it. [ToContinue](#)

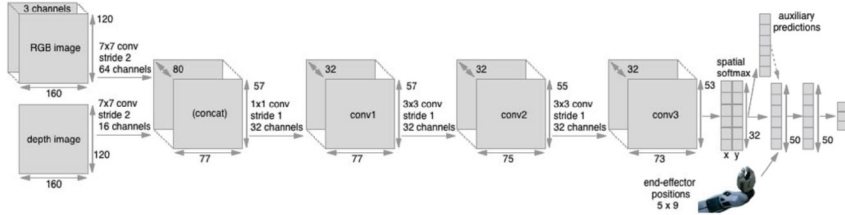


Figure 1.5: Architecture proposed in [4]

Table 1.1: Statistics of Training set, and Test Success rate [4]

Task	Reaching	Grasping	Pushing	Plane	Cube	Nail	Grasp-and-Place	Grasp-Drop-Push	Grasp-Place-x2	Cloth
#demo	200	180	175	319	206	215	109	100	60	100
demo duration (min)	13.7	11.1	16.9	25.0	12.7	13.6	12.3	14.5	11.6	10.1
Test success rate (%)	91.6	97.2	98.9	87.5	85.7	87.5	96.0	83.3	80.0	97.4

Interactive Imitation Learning

The Interactive Imitation Learning approach encompasses all methods specifically designed to address or mitigate the compounding-error phenomenon, which was first described in [42].

As previously mentioned, this problem arises from the fact that, while Behavioral Cloning (BC) primarily follows a supervised learning procedure, it does not satisfy the i.i.d. assumption. This is because the agent's actions influence subsequent observations, creating a dependency between samples in the training set. As a result, when the agent interacts with the environment, even small errors can lead to new observations that fall outside the training distribution, potentially leading to an unrecoverable situation that the robot cannot resolve autonomously.

The significance of this problem was first formalized in [53]. The authors observed that if a system makes an error with probability ϵ in a task with a time horizon of T , then, due to the compounding of

errors, a supervised learner incurs a quadratic total cost of $O(\epsilon T^2)$, instead of the expected linear cost of $O(\epsilon T)$. The quadratic term arises because, at any given time step t , the agent's state is influenced by errors made in the previous $t - 1$ steps. This cumulative effect breaks the independence assumption typically held in the i.i.d. setting.

To attenuate this problem, interactive supervised learning algorithms have been proposed, such as the well-known *DAgger* [54]. Algorithm 2 describes the DAgger procedure. It is an aggregation strategy, based on the idea to train the policy π^L under the state-distribution induced by the policy itself, but with the correct action performed by the expert. The main problem with DAgger is that it requires the expert to interact with the system during the training, introducing both **safety** and **data-efficiency** problems, especially when the system does not provide the human expert with sufficient control authority during the sampling process [55].

Algorithm 2 DAgger Algorithm [54]

Require: Initial Dataset $\mathcal{D} \leftarrow \emptyset$, Initial policy π_1^L

Ensure: The best policy π_i^L

for $i = 1, \dots, N$ **do**

 Sample $T - step$ trajectories using π_i^L

 Let $\mathcal{D}_i = (s_t, \pi^E(s_t))$, state s_t visited by policy π_i^L , and actions given by the expert

 Aggregate Dataset, $\mathcal{D} \leftarrow \mathcal{D} \cup \mathcal{D}_i$

 Train policy π_i^L on \mathcal{D}

 Let $\pi_{i+1}^L = \beta_i \pi^E + (1 - \beta_i) \pi_i^L$

end for

Human-Guided DAgger (HG-DAgger) [56] is an enhancement of the traditional DAgger strategy, where a human expert oversees the rollout of the current policy. If the agent moves into an unsafe region of the state space, the expert steps in to guide the system back

to safety. Specifically, HG-Dagger was proposed in the context of autonomous vehicle driving, however, in [13], it was shown that HG-Dagger is particularly effective in robotic manipulation tasks. The study found that, given the same total number of episodes, a policy trained exclusively on expert demonstrations has a significantly lower success rate than one trained on a dataset that includes both expert demonstrations and expert corrections.

In the context of Interactive Learning for Robot Manipulation, other works of interest include [57, 58].

In [58], a human expert provides both **corrective** and **evaluative** feedback. The former consists in the human that takes control of the robot to adjust the trajectory, the latter consists in a scalar weight q , set to 1 if the trajectory is satisfactory, 0 if the trajectory is not satisfactory, α if the trajectory is adjusted by the expert, where α is the ratio between non-corrected and corrected samples. Then a Neural Network was trained by minimizing a weighted version of the maximum-likelihood, $\mathcal{L}(a_t, s_t) = -q \log(\pi_\theta^L(a_t|s_t))$. Real-world experiments show that with a training time of **41 minutes**, including environmental reset, it was possible to have an agent capable of performing tasks such as picking up a cube or pulling a plug.

Multi-Task Imitation Learning

The methods discussed in the previous paragraphs describe architectures and approaches specifically designed to solve a single task, with limited generalization to the object’s category (e.g., picking blocks rather than balls) and initial state (e.g., the object’s starting position). For instance, a system trained for pick-and-place operations cannot be repurposed for tasks like assembly operations. The methods described in this paragraph address these limitations, solving the problem of *Multi-Task Imitation Learning* (MTIL)

Before starting to present and describe the different methods and

approaches, it is necessary to describe the problem. Starting from a reformulation of the dataset used to train the system and the learned policy. Indeed, in Section 1.3.1, the expert dataset \mathcal{D}^E has been introduced. Based on the problem to solve this dataset can be composed in different way. Specifically, in the context of MTIL, the dataset \mathcal{D}^E can be seen as a composition of n datasets, $\mathcal{D}^E = \{\mathcal{D}_1, \dots, \mathcal{D}_n\}$, where $\mathcal{D}_i = \{(\tau_{m_i}^j, c_{m_i}), j = 1, \dots, N, m_i \in \mathcal{M}_i\}$ is the *single-task dataset*, composed of:

- N expert demonstration for each m^{th} variation of the i^{th} task, where M_i is the number of variation for the i^{th} task.
- Agent trajectories $\tau_{m_i}^j = (s_0, a_0, s_1, a_1, \dots, a_{T-1}, s_T)$. where s_t is the state at time t and a_t is the corresponding action (Section 1.3.1).
- Task-conditioning signal c_{m_i} for the m^{th} variation of i^{th} task, which describes the desired task in terms of video demonstrations [12, 59, 6, 8], natural language description [9, 13, 10, 60, 61, 7, 14] or multi-modal prompt, that exploits both visual information (e.g., an image of the target object) and text information that contains the information related to the action to be performed [62].

The goal of Multi-Task Imitation Learning is to learn a *conditioned policy* $\pi_\theta^L(a_t|s_t, c_{m_i})$, that is able to map the current state and command into the corresponding action. Depending on how the policy is defined, various loss functions come into play. In the case of deterministic policies, the learning process focuses on minimizing the Mean-Squared Error (refer to Formula 1.6). However, for probabilistic policies, the learning process centers around minimizing the Negative Log-likelihood (refer to Formula 1.7). This approach aims to enhance the probability of correctly executing the action.

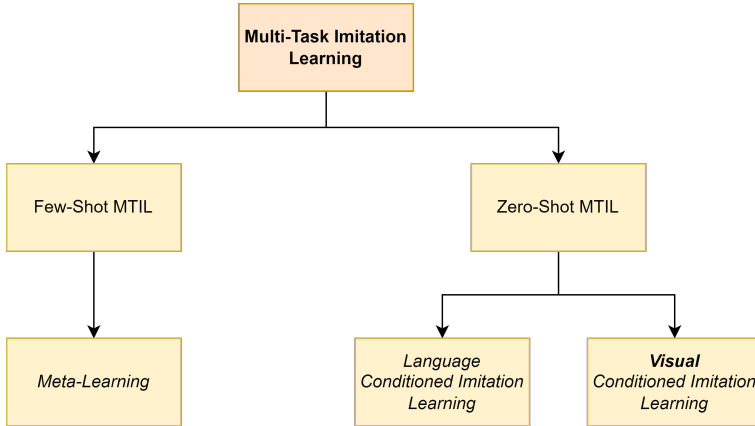


Figure 1.6: Multi-Task Imitation Learning Taxonomy

$$\mathcal{L}(\tau_{m_i}^j, c_{m_i}, \pi_\theta^L) = \frac{1}{T} \sum_{t=0}^T (a_t - \pi_\theta^L(s_t, c_{m_i}))^2 \quad (1.6)$$

$$\mathcal{L}(\tau_{m_i}^j, c_{m_i}, \pi_\theta^L) = -\frac{1}{T} \sum_{t=0}^T \log(\pi_\theta^L(a_t | s_t, c_{m_i})) \quad (1.7)$$

The following sections will describe the various approaches proposed to address the problem. Figure 1.6 illustrates the taxonomy used for the Multi-Task Imitation Learning methods. Specifically, the methods are categorized based on the type of generalization required by the algorithm (Few-Shot vs. Zero-Shot). For Few-Shot generalization, the Meta-Learning paradigm will be discussed, as it is most relevant to the problem at hand. For Zero-Shot generalization, the methods are further divided based on the type of conditioning signal used, whether it is provided through natural language descriptions or visual information.

Few-Shot MTIL refers to approaches designed to train a model

on a variety of tasks so that it can effectively solve a new task using only a small number of samples and consequently requires only a few back-propagation steps [63]. In this context, one of the most significant learning paradigms, especially relevant to robotic manipulation, is *Meta-Learning*. The goal of Meta-Learning is to train a model that can “learn to learn,” meaning it develops a set of general weights θ that, while not directly usable for solving any specific task within a distribution of tasks \mathcal{T} , can be quickly adapted through a few backpropagation steps to solve a given task within that distribution, $\mathcal{T}_i \in \mathcal{T}$. One of the most popular Meta-Learning algorithms is the *Model-Agnostic Meta-Learning* (MAML) algorithm [63], described in Algorithm 3. The MAML algorithm follows an iterative learning procedure consisting of two steps:

- **Meta-Learning:** During this phase, task-specific weights θ_i are computed for each sampled task \mathcal{T}_i . Specifically, the *meta-parameters* θ are updated according to the gradient obtained from evaluating the loss function on the i^{th} task \mathcal{T}_i , where the function f is parameterized by the meta-parameters θ .
- **Meta-Adaptation:** In this phase, the meta-parameters are further refined. The loss function f , now parameterized by the task-specific parameters for the i^{th} task, is used to adjust the meta-parameters based on the gradients derived from the sum of the loss functions evaluated on the task-specific weights. This process provides feedback to the meta-parameters θ from each task, leading to a generalized point that can be easily adapted to new tasks (Figure 1.7).

The MAML algorithm is the base for different methods which apply Few-Shot Imitation Learning in the context of Behavioral Cloning [64, 65, 66].

Algorithm 3 Model-Agnostic Meta-Learning (MAML) [63]

Require: Distribution over tasks $p(\mathcal{T})$
 Randomly initialize θ
while $i = 1, \dots, N$ **do**

 Sample batch of tasks $\mathcal{T}_i \sim p(\mathcal{T})$
for all \mathcal{T}_i **do**

 Evaluate $\nabla_{\theta} \mathcal{L}_{\mathcal{T}_i}(f_{\theta})$ w.r.t. K examples

 Compute adapted parameters with gradient descent: $\theta'_i = \theta - \alpha \nabla_{\theta} \mathcal{L}_{\mathcal{T}_i}(f_{\theta})$
end for

 Update $\theta \leftarrow \theta - \beta \nabla_{\theta} \sum_{\mathcal{T}_i \sim p(\mathcal{T})} \mathcal{L}_{\mathcal{T}_i}(f_{\theta'_i})$
end while

In [64], MAML algorithm was used to prove the effectiveness of Meta-Learning in the context of real robot manipulation, with visual observations, as opposite to [67]. A Convolutional Neural Network was trained by following the Algorithm 3, using as loss-function the Mean Squared Error, computed between the predicted action and the ground truth one. For real-robot experiments a dataset of **1300** placing demonstrations (i.e., place an holded object in a target container), containing near to **100** different objects, was collected through teleportation. The trained system was tested by performing the adaptation step on one video demonstration, over 29 new objects, moreover, between the video demonstration and the actual execution, the objects configuration was changed. In this setting the system reached the **90%** of success rate, outperforming baseline methods based on LSTM [67], and contextual network (i.e., a Convolutional Neural Network that takes in input the current observation and the image representing the target state).

In [65], the *Domain Adaptive Meta-Learning* algorithm (DAML) was proposed with the goal of learning to infer a policy from a single

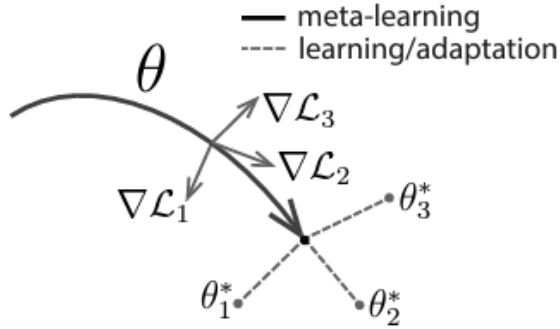


Figure 1.7: Diagram of MAML algorithm, which optimizes for a representation θ that can quickly adapt to new tasks

human demonstration. To achieve it, a two-step algorithm was proposed. In the first-step, called **Meta-Learning step**, given in input, for each task \mathcal{T} , a set of human demo $\mathcal{D}_{\mathcal{T}}^h$ and a set or robot demo $\mathcal{D}_{\mathcal{T}}^r$ (Figure 1.8), the *initial policy parameters* θ and the *adaptive loss* parameters ψ are learned, solving the problem in Formula 1.8.

$$\min_{\theta, \psi} \sum_{\mathcal{T} \sim p(\mathcal{T})} \sum_{\mathbf{d}^h \sim D_{\mathcal{T}}^h} \sum_{\mathbf{d}^r \sim D_{\mathcal{T}}^r} \mathcal{L}_{BC}(\theta - \alpha \nabla_{\theta} \mathcal{L}_{\psi}(\theta, \mathbf{d}^h), \mathbf{d}^r) \quad (1.8)$$

The outer loss is the classic supervised Behavioral Cloning loss, defined as $\mathcal{L}_{BC}(\phi, \mathbf{d}^r) = \sum_t \log(\pi_{\phi}(a_t \mid s_t, o_t))$. The inner loss, \mathcal{L}_{ψ} , is a learned **adaptive loss**. Specifically, \mathcal{L}_{ψ} is used during Meta-Adaptation, where the policy parameters are updated by evaluating the gradients derived from \mathcal{L}_{ψ} . This process involves using a video of a human demonstrating a new task \mathcal{T} as input, leading to the policy update defined by $\phi_{\mathcal{T}} = \theta - \alpha \nabla_{\theta} \mathcal{L}_{\psi}(\theta, \mathbf{d}^h)$.

This adaptive loss is the key component proposed in DAML. To use it effectively, it is necessary to learn the parameters ψ , observing how there is no direct correspondence between the human video demon-

stration and the robot’s ground truth actions. To address this challenge, the authors of DAML observed that while the policy learns to produce appropriate actions through the \mathcal{L}_{BC} loss, the adaptive loss should instead adjust the perceptual aspect of the policy, focusing on human motion and the manipulated object. Based on this insight, the authors implemented the function \mathcal{L}_ψ using a 1D Temporal Convolutional Network (Figure 1.9). The convolutional layers are applied to a stack of embeddings generated by the policy π across different frames of the video demonstrations. The parameters of this module are learned during the meta-training phase, following the weight update process described in Formula 1.9. The objective of \mathcal{L}_ψ is to generate task-specific policy parameters $\phi_{\mathcal{T}}$ that guide the policy to produce effective actions.

$$\begin{aligned} (\theta, \psi) &\leftarrow (\theta, \psi) - \beta \nabla_{\theta, \psi} \mathcal{L}_{BC}(\phi_{\mathcal{T}}, \mathbf{d}^r) \\ \phi_{\mathcal{T}} &= \theta - \alpha \nabla_\theta \mathcal{L}_\psi(\theta, \mathbf{d}^h) \end{aligned} \tag{1.9}$$

Experimental evaluation on tasks such as placing, pushing, and pick-and-place, has shown that:

- The system was able to generalize across both new objects and objects configuration starting from only a single human demonstration;
- A performance degradation was observed in large domain-shift experiments, such as novel backgrounds and different camera view-points.

Meta-Learning algorithms have demonstrated intriguing properties, notably their capacity for few-shot generalization to novel objects and object configurations. However, it has been observed that during the adaptation step, these methods tend to lose their effectiveness



Figure 1.8: Tasks performed in [65]. (Top row) Human demonstration, (Bottom row) robot demonstration. (Left) Placing task, (Middle) pushing task, (Right) pick-and-place task.

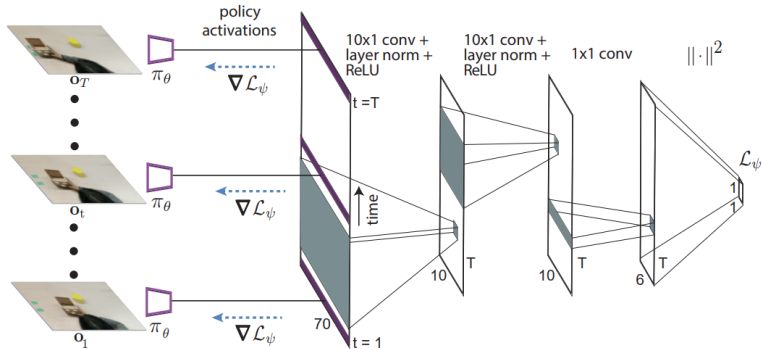


Figure 1.9: The Temporal Adaptation Loss architecture applies 1D temporal convolutional layers to the stacked embeddings generated by the policy π from the frames of the human video demonstration.

in performing other tasks. This limitation has underscored the need for the development of Multi-Task Imitation Learning methods, which aim to address these shortcomings and enable more versatile task execution in complex scenarios. These kind of methods will be discussed in the following paragraphs.

Zero-Shot MTIL refers to approaches that aim to train a model capable of solving different tasks without any further adaptation or backpropagation steps. This approach addresses a key issue in Meta-Learning methods, which is the problem of forgetting how to solve

previous tasks after adapting to a new one. The goal is to develop a single policy that can handle multiple tasks in a zero-shot manner.

In this context, a crucial design choice is how to convey the desired task to the policy. The literature identifies two main methods to address this problem:

1. *Language Conditioned*: These methods leverage natural language descriptions of tasks to inform the model about the task to be executed.
2. *Visual Conditioned*: These methods use visual information (e.g., goal-state images, video demonstrations) to provide the model with the task instructions.

Language Conditioned, as said a possible and intuitive way to inform the policy about which task to execute is through natural language description. Indeed, by looking to the phrase “Pick the blue cube and place it in the red bow”, there are both information about the action to perform (pick and place) and which are the objects involved (blue cube and red bow). Consequently, through training a neural network with a diverse set of tasks, the system should exhibit the ability to generalize its understanding to both previously unseen objects within familiar tasks and entirely novel tasks composed of the fundamental actions practiced during training. This approach showcases the potential for **robust** and **adaptable human-robot interaction** in real-world scenarios.

Foundational research, such as that by [9] and [13], has sought to explore the previously mentioned hypothesis. Notably, [9] introduced an innovative architectural framework, depicted in Figure 1.10, marking the first instance of seamlessly integrating language, vision, and control tasks. This model is composed of two critical components: a *Semantic Model*, which generates a task embedding denoted as e by

processing the initial scene image and the accompanying text command, and a *Control Model*, which generates the control signal using the current robot state r_t and the task embedding e .

A crucial aspect of such architectures is the management of the visual state, represented by the image I , and the command v , to create a meaningful embedding e that encapsulates both the current scene state and the desired command. Specifically, the image is first processed using a pre-trained object detection network (Faster R-CNN [68]) to identify salient objects in the robot’s environment. The detected objects are represented by feature vectors, which include class and bounding box information. Concurrently, the language command is embedded into a suitable representation using a language embedding technique (e.g., GloVe [69]), with the command vector V encoded by a recurrent GRU unit. To associate the objects identified with the sentence embedding s , a likelihood value is computed for each object proposal $a_i = w_a^T f_a([f_i, s])$, and a probability distribution is computed over the candidates $\mathbf{a} = \text{softmax}([a_0, \dots, a_c])$. Finally, the task embedding e is formed by a fully connected layer that takes as input the sentence embedding s and the weighted sum of object candidate features $e' = \sum_{i=0}^c f_i a_i$.

Training of this model was conducted on two fundamental tasks, namely “Picking” and “Pouring”, within scenarios featuring multiple objects of the same category, which served as distractors (see Figure 1.11). The subsequent testing experiments demonstrated the system’s capability to successfully complete the picking task 98 out of 100 times and the pouring task 85 out of 100 times within novel scenarios. These results serve as compelling evidence of the efficacy and potential of language-conditioned methodologies in the field.

Authors in [13] make a step towards a more general agent, by proposing a large-scale dataset containing **100** diverse manipulation tasks. The demonstrations were collected through both expert teleoperation and shared autonomy process (HG-DAgger [56]). The demon-

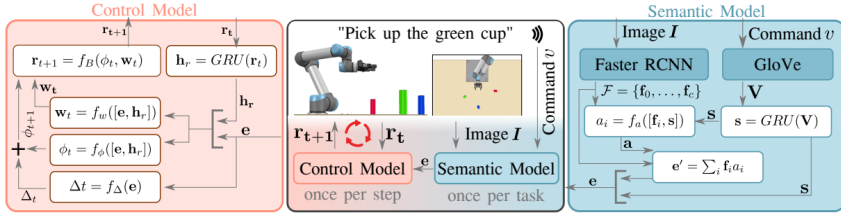


Figure 1.10: Architecture proposed in [9]. The *Semantic Model* takes in input the image I and the command v , generating a command conditioned embedding e . The *Control Module* receives in input the embedding e and the current robot state r_t and produces the next control signal.

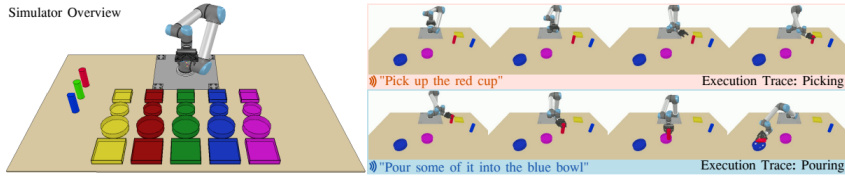


Figure 1.11: (Left) Set of object used in [9]. (Right) Sample of task execution (right)

strated tasks were related to pick-and-place, grasp, pick-and-drag, pick-and-wipe, and push skills. The dataset was used to train the network in Figure 1.12. As it can be noted the samples were composed by the current robot observation, and a conditioning represented by either a ***natural language description*** or a ***human video demonstration***. The idea was that training a conditioned policy over the current observation o_t , and a task representation c , , it would allow the policy to generalize over new tasks in a zero-shot manner (i.e., without any fine-tuning). Specifically, in contrast to the previous method, this approach does not rely on pre-trained object detectors to identify candidate regions. Instead, the Task Embedding is directly injected

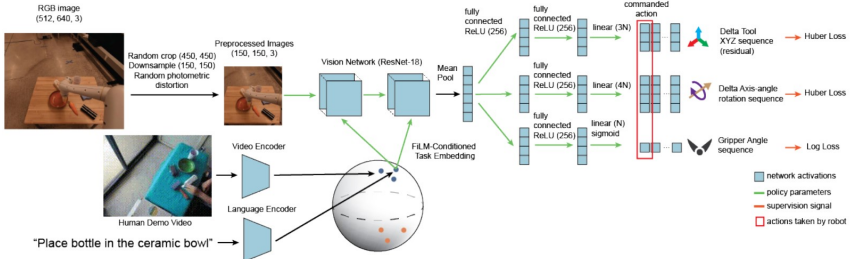


Figure 1.12: Architecture proposed in [13]. Here, the Task Embedding is injected directly in the Feature Maps generated by the Convolutional Neural Network ResNet-18. This injection is carried out through the FiLM layer [70].

into the Feature Maps generated by the Convolutional Neural Network ResNet-18. This injection is carried out through the FiLM layer [70].

Experimental results shown that, over 28 held-out tasks, containing both completely new objects, and known objects but in different tasks, an average success rate of **38%** was reached in the easiest setting, with only one distractor and with natural language instruction. The success rate dropped to **4%** in the hardest setting with 4 distractors and video conditioning.

Foundational research in the field of Language-Conditioned Multi-Task Imitation Learning has demonstrated promising results in zero-shot generalization. However, the robustness of their performance remains a challenge. Subsequent research, as highlighted in [7, 10, 61], has focused on enhancing performance.

In particular, the authors of [7] sought to investigate whether the transfer of knowledge from extensive, diverse, and task-agnostic datasets, which has enabled modern machine learning models to excel in zero or few-shot learning scenarios for new and specific tasks, is applicable within the realm of robotics. This inquiry arises due to the presence of high-capacity architectures capable of assimilating knowledge from such large datasets. To explore this prospect, the authors in [7] introduced a comprehensive dataset comprising

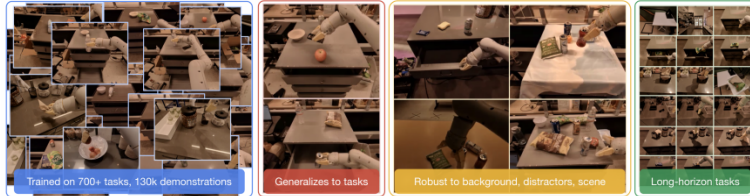


Figure 1.13: Examples of household scenarios in RT-1 large-scale dataset.

over 130,000 demonstrations collected across more than 700 household tasks (Figure 1.13). Additionally, they proposed a Language-Conditioned Transformer-based architecture (Figure 1.14). Here the authors made relevant modification in the architecture, with respect to the previous BC-Z architecture [13].Indeed, they modified the Visual Module by using an EfficientNet [71] instead of the ResNet-18. The instruction was encoded using the Universal Sentence Encoder [72], and the policy was implemented through a Transformer. Additionally, the authors addressed the real-time constraints of robot control. To accelerate inference time and achieve a frequency of 3 Hz, the authors employed a TokenLearner module [73], which utilizes an attention mechanism to select the most relevant tokens, thereby reducing the number of tokens that the underlying control module must process to infer the action.

It is worth noting the intriguing findings presented in Table 1.3. The model exhibits robustness in replicating tasks it has encountered before, and it even performs reasonably well on tasks it hasn't seen previously. However, a notable decline in performance becomes apparent when the model is exposed to novel backgrounds and scenarios featuring distracting objects, especially when the available data for these situations is limited. This observed trend holds significance because, unlike domains such as Computer Vision and Natural Language

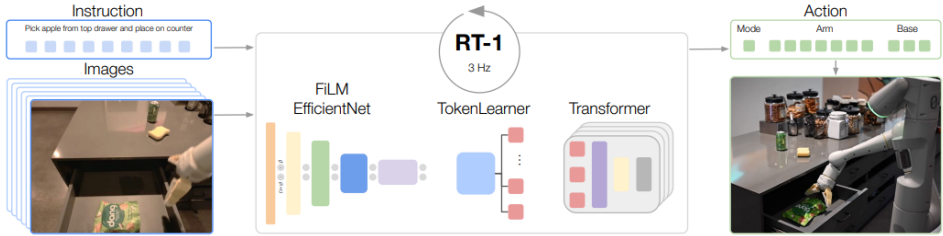


Figure 1.14: RT-1 Language-Conditioned Transformer based architecture proposed in [7].

Table 1.2: Distribution of tasks in large-scale dataset proposed in [7]

Skill	Count	Description	Example Instruction
Pick Object	130	Lift the object off the surface	pick iced tea can
Move Object Near Object	337	Move the first object near the second	move pepsi can near rxbar blueberry
Place Object Upright	8	Place an elongated object upright	place water bottle upright
Knock Object Over	8	Knock an elongated object over	knock redbull can over
Open Drawer	3	Open any of the cabinet drawers	open the top drawer
Close Drawer	3	Close any of the cabinet drawers	close the middle drawer
Place Object into Receptacle	84	Place an object into a receptacle	place brown chip bag into white bowl
Pick Object from Receptacle and Place on the Counter	162	Pick an object up from a location and then place it on the counter	pick green jalapeno chip bag from paper bowl and place on counter
	9	Skills trained for realistic, long instructions	open the large glass jar of pistachios pull napkin out of dispenser grab scooper
Total	744		

Processing where gathering large-scale datasets is relatively straightforward, the collection of real-world robotic datasets is a laborious and time-consuming endeavor. Furthermore, these real-world robotic datasets often have limited applicability to other research due to **disparities in action space, robot morphology, and scene representation**, as pointed out by [7]. Therefore, the aspiration is to develop a system capable of replicating tasks with minimal demonstrations specifically gathered from the particular robot in use.

Furthermore, the decline in success performance when faced with distractor objects emphasizes that addressing the policy-learning problem in an end-to-end manner, which involves mapping high-dimensional

Table 1.3: Results reported in [7] by training the same model RT-1 with different dataset size

Models	% Tasks	% Data	Seen Tasks	Generalization			
				All	Unseen Tasks	Distractors	Backgrounds
RT-1	100	100	97	73	76	83	59
RT-1	100	51	71	50	52	39	59
RT-1	100	37	55	46	57	35	47
RT-1	100	22	59	29	14	31	41

and high-level inputs like images and text directly to low-dimensional, low-level outputs such as the actions to be executed, may not be the most effective approach. This is because such models might lack the necessary perceptual components that enable them to initially recognize the target object within the scene, subsequently navigate towards it, and commence the manipulation process. This process aligns with how humans approach manipulation tasks [74].

As we have seen up to now, all the proposed methods were tested on different robotic platforms with different scenarios and environments. As in other Computer Vision problem, there are no well known benchmark that are used by the researchers around the world. To solve this problem, authors in [10] proposed CALVIN (Composing Actions from Language and Vision), which is an open-source simulated benchmark designed for learning long-horizon language-conditioned tasks in robotic manipulation. Specifically, CALVIN propose a set of 34 manipulation tasks in 4 different environments (Figure 1.15). This benchmark was used by [61, 75, 76]. Specifically, the work proposed in [76] is actually the best performing method on the CALVIN benchmark. The authors proposed an architecture that is able to handle goals described in terms of both natural language description and goal image, moreover they used a Diffusion Transformer Model as policy (Figure 1.16). To reach this goal, the authors had to solve first of all the problem related to how to force the Multimodal Transformer

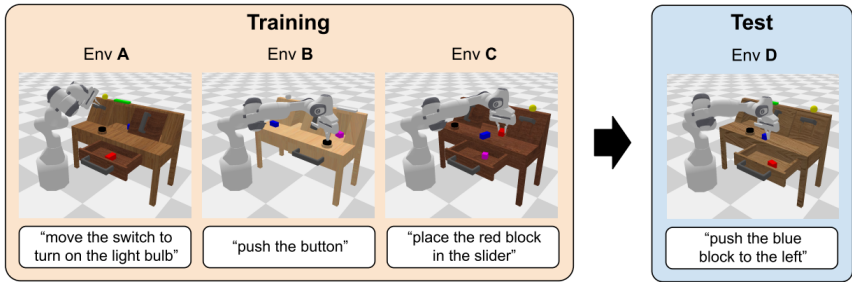


Figure 1.15: Environment proposed in CALVIN benchmark [?]. The environments have different textures and all static elements such as the sliding door, the drawer, the light button, and switch are positioned differently

Encoder to generate the same behavior independently from the goal modality. To solve this problem authors of MDT proposed two auxiliary self-supervised loss functions:

- *Masked Generative Foresight* (MGF) is a reconstruction-loss function designed to ensure that the MDT generates embeddings capable of guiding the robot behavior consistently across different modalities. This means that the tokens generated by the MDT can be used to construct image patches representing feature states, whether the goal is specified in terms of an image or a language description. Specifically, given the latent embedding of the MDT encoder for state s_i and goal g , MGF trains a Vision Transformer (ViT) to reconstruct a sequence of 2D image patches $(u_1, \dots, u_U) = \text{patch}(s_{i+v})$ corresponding to the future state s_{i+v} .
- *Contrastive Latent Alignment* (CLA) is a contrastive loss term designed to encourage the MDT to align the embeddings generated from a goal image with those generated from a language

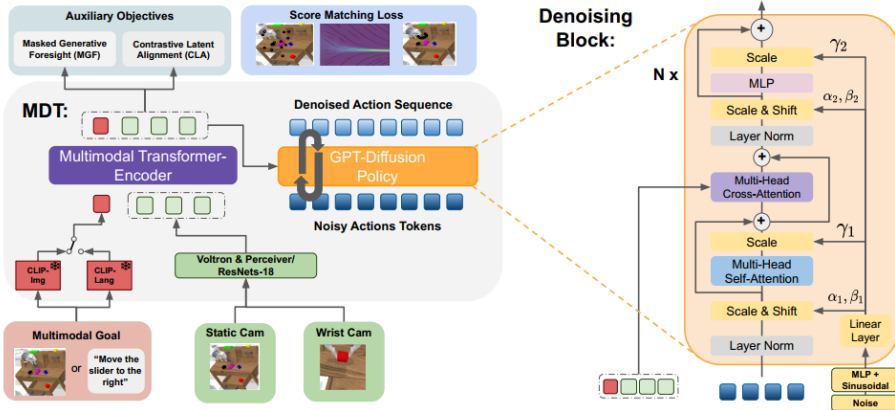


Figure 1.16: The Multimodal Diffusion Transformer (MDT) architecture proposed in [76]

description. For each training sample (s_i, a_i) paired with a multimodal goal specification $G_{s_i, a_i} = \{o_i, l_i\}$, CLA reduces the image and language goals to vectors z_i^o and z_i^l , respectively. The CLA loss is then computed using the InfoNCE loss, based on the cosine similarity $C(z_i^o, z_i^l)$ between the image-goal conditioned state embedding z_i^o and the language-goal conditioned state embedding z_i^l .

As mentioned, this method was tested on the CALVIN benchmark, specifically in the $ABCD \rightarrow D$ test scenario, where the model was trained on the $ABCD$ environments and tested on environment D . The CALVIN benchmark comprises a set of 1000 rollouts, with each rollout consisting of a sequence of 5 commands. It is noteworthy that the MDT architecture successfully completed 80% of the rollouts up to the fifth command. In particular, the MGF loss was observed to have a significant impact on system performance, improving the success rate for the fifth command from 69.8% to 79.4%. This demonstrates that

making the embedding informative about the system’s evolution can meaningfully guide the diffusion system, which predicts actions over a certain time horizon into the future.

In the context of Language Conditioned MTIL, other important works to cite include [77, 14]. Specifically, the authors in [77] introduced CLIP-Port, a two-stream architecture that explicitly models the two key tasks in language-conditioned imitation learning: reasoning about **what to do** and reasoning about **how to do it**. The former task, referred to as *semantic reasoning*, is derived from the text-based command and is handled using a pre-trained CLIP architecture [78]. The latter task, known as *spatial reasoning*, is managed by leveraging the Transporter architecture [79]. The overall architecture (Figure 1.17) is an Encoder-Decoder framework that ultimately outputs an **affordance map**, which identifies the locations for executing pick or place operations (Figure 1.18).

During testing, this method was not directly compared with other Language Conditioned MTIL approaches. However, the results obtained allow for several observations. Notably, for tabletop manipulation tasks, the ability to reason using both spatial and semantic features enables a high success rate (ranging from 80% to 90%) on tasks involving seen object attributes, such as color, even with a relatively low number of demonstrations (100). However, similar to the results reported in Table 1.3, CLIP-Port also struggles with entirely novel tasks, as evidenced by a significant drop in performance when dealing with unseen object attributes and a lower number of demonstrations.

In conclusion, as discussed in this paragraph, considerable research effort has been dedicated to addressing the problem of Language Conditioned MTIL, particularly in terms of architectural designs and learning strategies. However, it remains challenging to draw definitive conclusions from these various approaches, as they are generally not evaluated on a common benchmark. Despite this issue, some trends can

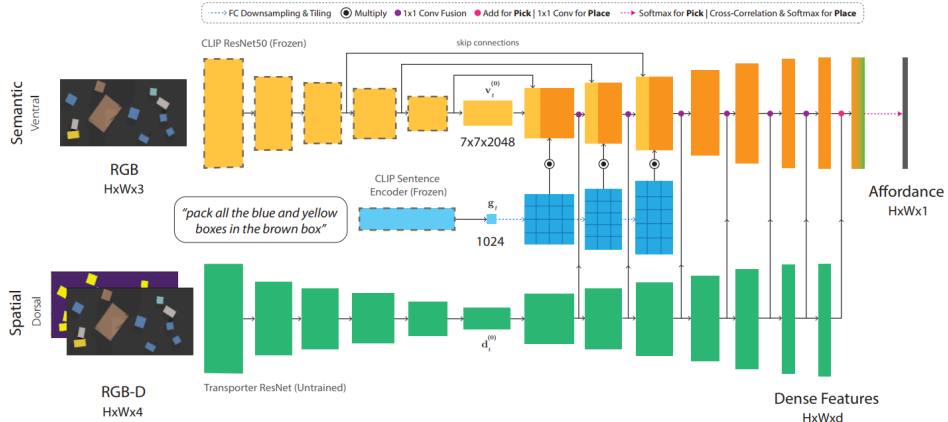


Figure 1.17: The Dual Stream architecture proposed in [77] consists of two parallel streams: a semantic stream and a spatial stream. The semantic stream utilizes a frozen CLIP ResNet50 to encode the RGB input, with the decoder layers conditioned by tiled language features from the CLIP sentence encoder. Meanwhile, the spatial stream encodes the RGB-D input, and its decoder layers are laterally fused with those of the semantic stream. The final output is a map of dense pixelwise features, which is used to predict pick or place affordances.

be observed. There is clearly room for improvement in the generalization capabilities of these methods, particularly in handling novel scenarios and tasks. Additionally, data efficiency remains a concern, as there is a noticeable decline in performance as the number of expert trajectories decreases. Another challenge is the ability to manage cluttered scenes with **relevant distractors**, objects that may have been manipulated during training but must be ignored in the target task, which can lead to occlusion and/or confusion.

Visual Conditioned refers to methods that use visual information as a conditional signal. This information can be represented either as



Figure 1.18: Example of affordance map. (Left) The top-view input image. (Center) The affordance map for the pick-operation, since the task is to grab cherries the map highlights the two pickable cherries. (Right) The affordance map for the place operation.

an image depicting the desired goal state or as a sequence of frames illustrating how the task should be performed. The idea behind this kind of methods is to build systems that are able to replicate tasks by observing the execution performed by other agents, like human can learn task by mimiking the execution of other humans.

Preliminary works, such as those by [12] and [59], introduced architectures conditioned on the first and last frames of task demonstrations. Specifically, in [12], the authors proposed TecNets (Task-Embedded Control Networks), an architecture illustrated in Figure 1.19. TecNets consist of two main components:

- *Task-Embedding Network*: The purpose of this network is to create an embedding space where demonstrations of the same task are closely clustered, while embeddings of different tasks are kept as distant as possible. This network is trained using a contrastive loss function, defined in Formula 1.10, which ensures that the embedding of the k^{th} sample of the j^{th} task is similar to the "sentence" representing that task (i.e., the average of the embeddings of the j^{th} task) and maximizes the distance from

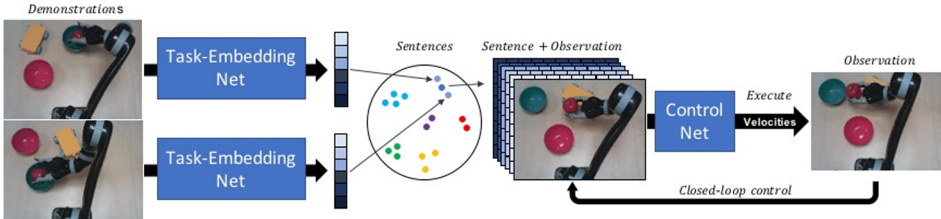


Figure 1.19: Architecture proposed in [12]. The *Task Embedding Net* generates the embedding representing the task to be performed given the goal image. The *Control Net* implements the policy, and takes in input the current observation and the tiled task embedding

the sentences of other tasks.

$$\mathcal{L}_{emb} = \sum_{\tau_k^j \in \mathcal{T}^j} \sum_{\mathcal{T}^i \notin \mathcal{T}^j} \max [0, \text{margin} - s_k^j \cdot s^j + s_k^j \cdot s^i] \quad (1.10)$$

- *Control Network*: This module implements the policy π , which takes as input the current observation o and the sentence s of the desired task. It then generates the corresponding action for the robot, conditioned on the task.

The results from this preliminary work demonstrated the feasibility of training a vision-conditioned system capable of solving tasks in a zero-shot manner. The system achieved a success rate of **86.31%** on a simulated 2D reaching task and **77.25%** on a simulated pushing task. However, it is important to note a significant limitation of these approaches: the conditioning signal often fails to adequately capture critical information about the optimal strategy for solving the task. This shortcoming arises because the conditioning signal does not fully encode the strategies needed for effective task execution.

The methodologies introduced in [6] and [8] aim to advance the concept of an ideal multi-task agent, capable of replicating new tasks

based on a single demonstration, often performed by another agent (e.g., a robot or a human).

In [6], the authors focused on training a vision-based control architecture (depicted in Figure 1.20) that can replicate a task demonstrated through a set of frames sampled from a video of another agent performing the task. The architecture relies on two main components:

- *ResNet-18* [80], which serves as the backbone for extracting visual embeddings from the current agent state and the demonstration frames.
- *Transformer* [81], which uses the attention mechanism to combine embeddings from the demonstration frames with the current visual observation.

This architecture was trained using multiple loss terms, specifically:

- *Behavioral Cloning* term \mathcal{L}_{BC} (Formula 1.11), a supervised loss function used to learn the action to perform given the agent's observation and the demonstrated task. Specifically, the loss function is a negative log-likelihood, computed over a mixture of learned logistic distributions, where the i^{th} component is parameterized according to the mean and variance (μ_i, σ_i) which are estimated through a MLPs.

$$\mathcal{L}_{BC} = -\ln\left(\sum_{i=0}^k \alpha_i(\phi_t) P(a_t, \mu_i(\phi_t), \sigma_i(\phi_t))\right) \quad (1.11)$$

- *Inverse Model Regularizer* term \mathcal{L}_{inv} (Formula 1.12), a regularization term where the output is the action a_t , given two consecutive representations $\tilde{\phi}_t$ and $\tilde{\phi}_{t+1}$, effectively solving the inverse

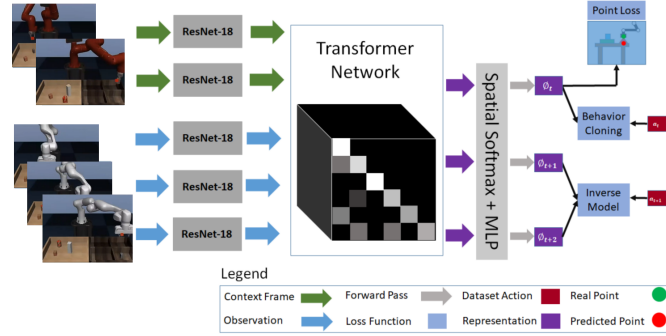


Figure 1.20: Transformer based architecture proposed in [6]. The Transformer network is used to create task-specific representation, given context and observation features computed with ResNet-18.

control problem.

$$\mathcal{L}_{inv} = -\ln\left(\sum_{i=0}^k \alpha_i(\tilde{\phi}_t, \tilde{\phi}_{t+1}) \text{logistic}(\mu_i(\tilde{\phi}_t, \tilde{\phi}_{t+1}), \sigma_i(\tilde{\phi}_t, \tilde{\phi}_{t+1}))\right) \quad (1.12)$$

- *Point Prediction Auxiliary* term \mathcal{L}_{point} , a simple regression loss that, given the current representation ϕ_t , predicts the position of the gripper in the next $t + H$ steps. This loss is used to improve the explainability of the actions performed by the robot.

The authors specifically trained and tested the architecture on the *pick-place* task, which consists of a total of 16 variations (Figure 1.21). In the proposed evaluation setting, the TOSIL architecture achieved a success rate of **88.8% \pm 5.0%**, demonstrating the system’s ability to accurately capture the requested variations represented in the demonstration frames, even when faced with differences in robot embodiment.



Figure 1.21: Validation setting proposed in [6]. The 16 tasks consist of taking an object (a-b) to a bin (1-4). On the left there is the demonstrator robot, while on the right there is the agent robot.

In [8], the authors presented MOSAIC (Multi-task OneShot imitation with self-Attention and Contrastive learning), which is an improvement of the work proposed in [6] from both the architectural point-of-view and from the evaluation setting. Indeed, from the architectural point of view, MOSAIC is designed to model a demonstration-conditioned policy, denoted as $\pi_\theta^L(a_t|s_t, c)$, with c representing the current task demonstration, such as a video depicting a robot performing the task. Specifically, the architecture is an optimization of TOSIL since, where the encoder-decoder Transformer architecture has been substituted with an encoder-only architecture leveraging the self-attention mechanism to correlate the embeddings coming from the current agent observation and the one coming from the demonstration frames (Figure 1.22). This adjustment allows to have a lower number of parameters and consequently improve the inference time.

To handle this complex scenario involving both multiple variations and multiple tasks, the authors proposed training the system using a combination of loss functions. Specifically, in addition to the \mathcal{L}_{BC} loss function defined in Formula 1.11 and the \mathcal{L}_{inv} loss function defined in Formula 1.12, the authors introduced a contrastive loss term implemented through the InfoNCE objective (Formula 1.13). The goal of this loss is to enable the system to create similar representations for time-adjacent frames within a given task while maximizing the

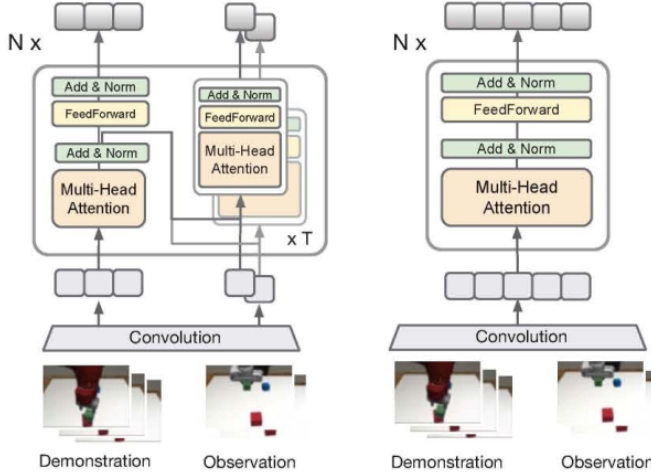


Figure 1.22: (Left) The TOSIL architecture, as proposed in [6]. (Right) The MOSAIC architecture, as introduced in [8]. In the MO-SAIC architecture, the original encoder-decoder Transformer architecture has been replaced with an encoder-only architecture featuring self-attention modules.

distance from representations corresponding to other tasks. In this context, q is the anchor embedding obtained from a randomly sampled frame in a given batch B , k_+ is the positive example, which is a nearby frame from a different view of the batch (i.e., the original batch with a different data augmentation applied), and k_i represents the negative samples, obtained from any other frame in the batch.

$$\mathcal{L}_{Rep} = \log \left(\frac{\exp(q^T W k_+)}{\exp(q^T W k_+) + \sum_{i=1}^{F-1} \exp(q^T W k_i)} \right) \quad (1.13)$$

To test the model, a dataset containing **seven distinct tasks** and **61 variations** (Figure 1.23) was generated by executing hand-written



Figure 1.23: The evaluation tasks proposed in [8] consist of a total of 7 tasks with 61 semantic variations.

policies in a simulation environment. This dataset was employed to train and compare the proposed MOSAIC architecture against other one-shot (meta-)imitation learning methods, such as [65] and [6]. The results, presented in Table 1.4, demonstrate that MOSAIC surpasses previous methods in the Single-Task Zero-Shot Imitation Learning setting, particularly when addressing individual tasks with multiple variations and testing on previously unseen scenarios (i.e., novel object configurations).

Furthermore, when evaluated in a Multi-Task setting, where the system is trained on all tasks and subsequently tested on each task separately, MOSAIC exhibits the capability to partially replicate the demonstrated tasks. It is important to note that transitioning from a single-task to a multi-task context introduces inherent challenges. Despite being familiar with the tasks used during training, the success

Table 1.4: Results obtained in single-task and multi-task one-shot imitation learning [8].

Task	Setup	DAML [65]	TOSIL [6]	MOSAIC [8]
Open door	single	23.3 ± 5.2	57.9 ± 7.1	67.1 ± 5.5
	multi	10.8 ± 5.4	49.2 ± 6.0	68.3 ± 6.3
Open drawer	single	15.4 ± 5.5	57.5 ± 3.9	65.4 ± 3.4
	multi	3.3 ± 1.4	53.3 ± 4.0	55.8 ± 3.6
Press button	single	62.8 ± 3.9	56.4 ± 2.4	71.7 ± 3.9
	multi	1.7 ± 0.7	63.3 ± 3.5	69.4 ± 3.4
Pick-and-Place	single	0.0 ± 0.0	74.4 ± 2.1	88.5 ± 1.1
	multi	0.0 ± 0.0	19.5 ± 0.4	42.1 ± 2.3
Stack block	single	10.0 ± 1.8	13.3 ± 2.6	79.3 ± 1.8
	multi	0.0 ± 0.0	34.4 ± 3.4	70.6 ± 2.4
Basketball	single	0.4 ± 0.3	12.5 ± 1.6	67.5 ± 2.7
	multi	0.0 ± 0.0	6.9 ± 1.3	49.7 ± 2.2
Nut assembly	single	2.2 ± 1.4	6.3 ± 1.9	55.2 ± 2.8
	multi	0.0 ± 0.0	6.3 ± 1.3	30.7 ± 2.5

rate tends to decrease for almost all tasks. This phenomenon underscores the necessity for training procedures and architectures capable of generating embeddings that accurately represent both the task itself and its various sub-tasks. Such capacity is essential for reusing these embeddings when executing new instances or entirely novel tasks.

In this context, further improvements were introduced by the authors of [23, 82]. Specifically, the authors in [23] analyze the shortcomings of existing methods like TOSIL and MOSAIC, which often struggle due to issues such as the DAgger problem (distribution shift from offline training), last-centimeter errors in fine motor control (e.g., collisions when the robot reaches the target object to pick), and misalignment with task contexts rather than the actual tasks (e.g., the system links the trajectories to the objects present in the scene rather

than focusing on what is demonstrated by the expert).

To overcome these issues, the authors proposed a modular approach that separates task inference, i.e., understanding the intent of the demonstrations, from task execution, i.e., generating the actions to perform during the rollout. To achieve this, they introduced AWDA (Attributed Waypoints and Demonstration Augmentation), a modular framework for visual demonstration represented in Figure 1.24. AWDA is based on two main concepts:

- *Attributed Waypoints*, designed to mitigate task execution errors, primarily those related to the distributional shift problem. These are classic waypoints (i.e., sequences of 6D poses of the end-effector) augmented with attributes, such as whether there is an object in the gripper. The robot moves between these generated waypoints using hand-defined motion primitives, which helps eliminate small errors during rollout execution that could otherwise cause the system to deviate from the correct trajectory.
- *Demonstration Augmentation*, introduced to decouple tasks from task contexts. Specifically, two types of augmentation are introduced: **Asymmetric Demonstration Mixup**, which generates novel samples by mixing samples from two distinct trajectories according to Formula 1.14, where v and \tilde{v} are video demonstrations of two distinct tasks, and o and \tilde{o} are agent observations in two distinct contexts. **Additional Demonstrations via Trajectory Synthesis** involves generating free-space motions for the robot in various contexts by sampling a small number of points (1 to 3) uniformly at random within the agent’s workspace and moving the end effector sequentially through these points using an inverse kinematics solver. Training samples are created by pairing each trajectory with itself, requiring the model to fo-

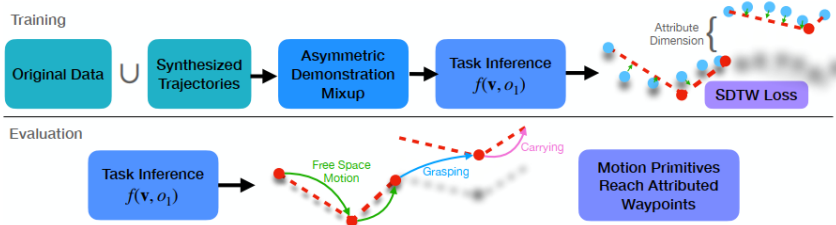


Figure 1.24: AWDA framework proposed in [23]. The task inference network $f(v, o)$ predicts a sequence of attributed waypoints (red dots) that are achieved by hand-defined motion primitives. The original data are augmented with free-space motion trajectories and asymmetric demonstration mixup in order to reduce the correlation between tasks and task content.

cus on the motion of the arm and ignore background elements to make correct predictions.

$$v'_t = \alpha v_t + (1 - \alpha) \tilde{v}_0 \quad o'_t = \alpha o_t + (1 - \alpha) \tilde{o}_0 \quad (1.14)$$

Using this framework, the authors trained the same Transformer-based architecture as in [6], achieving notable results. Specifically, on the pick-place task represented in Figure 1.21, AWDA reached a success rate of **100%** on two held-out variations, i.e., the system was trained on 14 variations and tested on the remaining 2. However, when tested on completely novel tasks, i.e., tasks never seen during training, the system struggled to succeed, as reported in Table 1.5.

In conclusion, significant research efforts have been dedicated to addressing the challenge of Visual Conditioned Multi-Task Imitation Learning (MTIL). The aim is to develop systems capable of solving a given task in a zero-shot manner, starting from just a single video demonstration. Specifically, while these systems show promising results in solving new instances of seen tasks and unseen variations of

Table 1.5: Success rates achieved using the MOSAIC and AWDA methods. In this scenario, training is conducted on 5 out of the 6 tasks, with the remaining task reserved for testing.

	Door	Drawer	Button	Blocks	Basketball	Nut Assembly
MOSAIC	0.05	0.15	0.05	0	0	0
AWDA	0.10	0.29	0.01	0	0	0.02

known tasks, they struggle to handle a multi-task multi-variation setting, exhibiting a consistent drop in performance. Additionally, they face difficulties in solving entirely new tasks.

Furthermore, the work discussed in this section predominantly involves experiments conducted in simulation environments, leaving unanswered the question of whether these systems can be effectively applied in real-world settings, where demonstrations might also come in the form of human video demonstrations.

Object-Oriented Imitation Learning

All the methods discussed so far share a common characteristic: they are end-to-end systems that take high-level inputs, such as images, and directly generate the corresponding actions as output. While this approach can be sufficient in scenarios where the scene is simple, meaning there are no distracting objects, or if there are distracting objects, they can be easily identified by the system because they are consistently not involved in the manipulation, this end-to-end approach may struggle in more complex environments. Specifically, it can encounter difficulties when the robot workspace contains objects that are similar to each other, especially if these objects are involved in manipulation for some task variations.

Based on this consideration, this paragraph will describe methods that leverage **object priors**. Specifically, leveraging object priors means that the control policy is informed not only by the embedding

of the agent scene, which is obtained from a deep architecture, but also by object-level information, such as the bounding boxes of objects in the scene, obtained from an object detector.

The concept of leveraging object priors has been explored in both earlier works [83, 84] and more recent approaches [85, 86, 87, 62].

One of the preliminary works on leveraging object priors was presented by the authors of [83]. This work primarily focuses on the challenge of generalization in Learning from Demonstration (LfD) systems that use an end-to-end approach. In such systems, a task-specific model is trained to predict actions based on raw visual observations. The authors found that while it is possible to achieve good *instance-level generalization*, meaning the model can solve tasks with varying initial configurations using a limited number of samples, achieving *category-level generalization* is more challenging. Category-level generalization refers to the model ability to solve tasks involving different objects. To achieve this, the dataset must include a large number of trajectories involving a wide variety of objects. For instance, if the task is to pour the contents of a bottle into a cup, the dataset should contain trajectories with different types of cups and bottles. However, constructing such a dataset is time-consuming and costly. Moreover, the potential of well-known large datasets in classical computer vision tasks, such as object detection, is not fully utilized.

To address this issue, the authors proposed a paradigm shift by introducing a robotic vision framework that operates on sets of objects rather than raw pixel data. This framework leverages prior datasets to learn a generic object concept model, thereby enhancing category-level generalization without requiring an extensive and diverse dataset. The framework is illustrated in Figure 1.25 and is composed of several stages:

- **Meta-Attention**, which is basically a Region Proposal Network (RPN) [68], trained on the well known MSCOCO [88] dataset.

The RPN generates objects proposals, i.e., region of the image that possibly contain an object.

- **Task-Specific Attention**, which aims to learn what are the object of interest with respect to the task in hand. This module is parametrized as a vector w such that the attention paid to o^i is proportional to $e^{w^T f(o^i)}$.
- **Soft Attention**, this module gives a probabilistic meaning to the attention map obtained from the Task-Specific Attention. Specifically, a Boltzmann distribution is used to map the attention weights to a probability for each object proposal, i.e.,

$$p(o^i | w_j) = \frac{e^{w_j^T \frac{f(o^i)}{\|f(o^i)\|_2}}}{\sum_{i=0}^N e^{w_j^T \frac{f(o^i)}{\|f(o^i)\|_2}}}.$$

- **Movement Prediction Network**, this module predicts the next robot action, given the attended object information from the soft attention, and the robot state represented by the joint and end-effector state.

This preliminary work focused mainly on two tasks:

- *Pouring Task*: The robot is required to pour contents from a bottle into a mug. The challenge is to locate the mug from an image without being explicitly provided its location, especially when different mugs are used during training and testing.
- *Sweeping Task*: The robot must sweep an object (e.g., a plastic orange) into a dustpan, with both objects starting in different positions. This task requires the robot to adapt its approach based on the relative positions of the objects. During testing, the authors focused on *Category Generalization* and the ability to *Ignore Distractor Objects*. For the former, the system was trained with only one type of mug and evaluated with other mugs (Figure 1.26). The results showed that the system successfully poured the contents

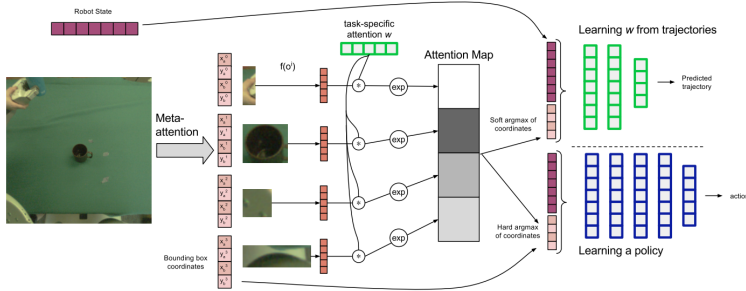


Figure 1.25: Robotic vision framework proposed in [83]. The framework is divided into different stages: **Meta-Attention**: Generates object proposals from an input image, trained on an object detection dataset, and shared across tasks; **Task-Specific Attention**: Focuses on relevant objects for a task using the meta-attention’s semantic features; **Soft Attention**: Distributes attention as probabilities over object proposals using a Boltzmann distribution; **Movement Prediction Network**: Combines attended object information with the robot’s state to predict the next action.

into the correct mug, thanks to the learned task-specific attention weight that highlighted the mug features. For the latter, the authors designed a test where two mugs were present in the scene (Figure 1.27). Since the model did not receive any conditioning signal indicating which mug to use, the authors fine-tuned the attention weight on trajectories where only the brown mug was used, demonstrating that this mechanism could focus on more specific features, such as the mug color.

In summary, this preliminary work demonstrated that leveraging object priors can facilitate category-level generalization by utilizing large, well-known datasets for the object-detection problem. However, the experimental setup was relatively simple, even in scenarios



Figure 1.26: Pouring task setting proposed in [83]. (Left) Mugs used for evaluation. Note that only the brown mug was seen during training. Center: Successful pouring into the pink mug. (Right) Pouring into the brown mug in a cluttered environment that was not seen during training.

with distractor objects. The proposed system could handle distractor objects only after specific fine-tuning and was not able to dynamically discriminate between objects of interest and distractors based on task variations.

A recent work that follows a similar approach is proposed in [86]. In this work, the authors introduced VIOLA (Visuomotor Imitation via Object-centric Learning) (Figure 1.28), an architecture inspired by the ideas presented in [83]. VIOLA uses an RPN and a ResNet18 [80] to generate object proposals and produce a spatial feature map, respectively. It then constructs a *per-step feature* vector, composed of three key elements: a **global context feature** that encodes the current task stage, an **eye-in-hand visual feature** to mitigate occlusion, and a **proprioceptive feature** that captures the robot state. These per-step features are concatenated to form a **history of observations**, which is designed to capture temporal dependencies and dynamic changes in object states. This tensor is then fed into a Transformer [81], which leverages its intrinsic attention mechanism to automatically focus on the object of interest.

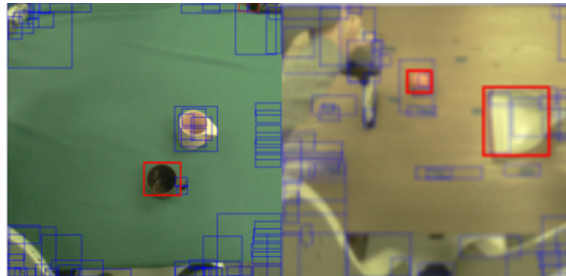


Figure 1.27: The region proposals (meta-attention) are drawn in blue and the task-specific attended regions are drawn in red. For the Pouring task with distractor mug (pink) and target mug (brown), the attention locks on to the brown mug as its position defines the trajectory. For the sweeping task, two attention vectors are used, one attends to the orange and one attends to the dustpan.

This method was first evaluated in a simulation environment across three tasks, as depicted in Figure 1.29. Various testing scenarios were considered, including different object placements, the introduction of distractor objects, and changes in camera position. Generally speaking, VIOLA outperformed all baselines across these testing conditions, further demonstrating the utility of object priors in enhancing the robustness of such methods. However, similar to [83], the testing scenarios were relatively simple, with clear distinctions between distractors and objects of interest. The distractors were objects never seen during the demonstration and were not involved in manipulation, making them relatively easy for the model to discriminate.

In the works discussed so far, the approach has primarily focused on leveraging object priors to directly predict the actions that the robot must perform. However, a different approach was proposed in [85], where the authors introduced an alternative interpretation of object-centric concept. Instead of focusing on the robot perspec-

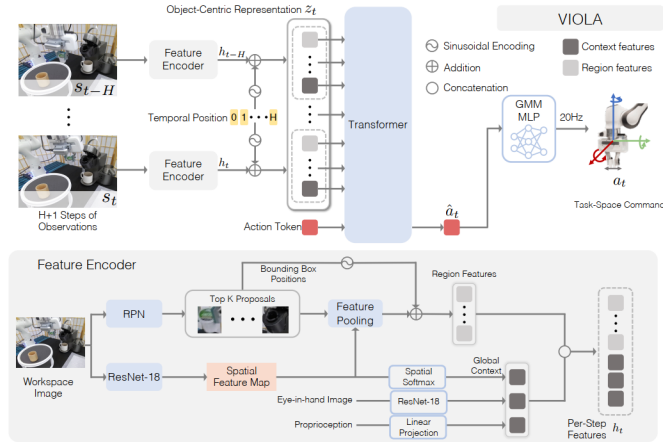


Figure 1.28: VIOLA architecture proposed in [86].

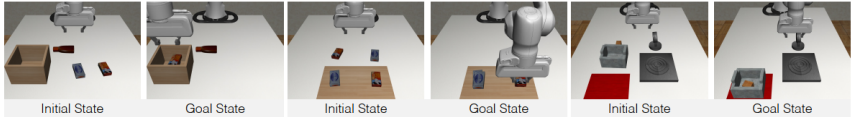


Figure 1.29: Simulation tasks on which the VIOLA [86] method was tested. (Left) Sorting task. (Center) Stacking task. (Right) BUDS-Kitchen task

tive, they shifted the emphasis to the object perspective, proposing PLATO (Predicting Latent Affordances Through Object-Centric Play). PLATO is a learning framework that learns a **latent affordance space**, which describes how an object can be used (e.g., a block being grasped, a door knob being turned, or a drawer being opened).

The authors argue that learning these affordances (i.e., what happens to the object) rather than plans (i.e., what happens to the robot) from play leads to a simpler and more robust task representation that can operate over varying time horizons. This, in turn, results in more

effective policies at test time. This paradigm shift allows the policy to reason about the environment more effectively: given access to an affordance (e.g., the door knob being turned) and a goal (e.g., an opened door), the policy can work backwards to infer the behavior needed to exploit that affordance (e.g., reaching the knob and rotating the gripper to turn it).

To reach this objective authors started from the observation that a single-object manipulation is composed of the following three phases:

1. **Pre-interaction**, when the robot prepares to interact with an object (e.g., reaching for a block).
2. **Interaction**, when the robot and the object engage in joint actions (e.g., pushing or pulling the block).
3. **Post-interaction**, when the robot separates from the object, and the object may come to rest (e.g., the block stops moving).

Given these three phases, the algorithm learns a **latent affordance distribution**. Specifically, the architecture comprises three learnable modules: E , E' , and π . E models the posterior distribution, mapping the full interaction trajectory τ^i to the corresponding latent affordance distribution, from which the affordance embedding z is sampled. E' is the prior module used during rollout. It takes the current state and the goal state as input and generates the affordance embedding z' . This module is trained to match the posterior distribution modeled by E . π represents the current policy, which generates the action a^i given the current state s^i , the desired goal o_g , and the latent embedding z .

These three modules are trained end-to-end by minimizing the loss function in Formula 1.15, which includes three terms. The first two terms correspond to the policy π , ensuring it matches the ground-truth trajectories in the interaction and pre-interaction phases. The last term is the KL-divergence, used to train the posterior and prior modules E and E' .

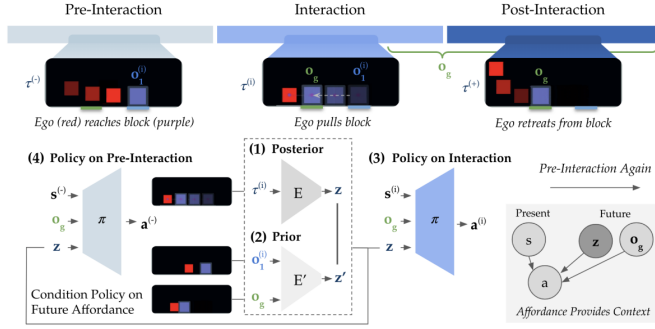


Figure 1.30: PLATO architecture proposed in [85]. The architecture is composed of different stages. (1) The posterior encoder E encodes the interaction sequence $\tau^{(i)}$ into the affordance z . (2) The prior encoder E' encodes the object initial state $o_1^{(i)}$ and goal state o_g to predict z , with o_g sampled after the interaction. (3) The policy is trained to output actions during the interaction period conditioned on the affordance. Simultaneously, (4) it is trained to output actions during the pre-interaction period conditioned on the “future” affordance.

$$\begin{aligned} \mathcal{L}_{PLATO} = & -\log \left(\pi \left(a_{1:H}^{(i)} \mid s_{1:H}^{(i)}, o_g, z \right) \right) - \\ & \alpha \log \left(\pi \left(a_{1:H}^{(-)} \mid s_{1:H}^{(-)}, o_g, z \right) \right) + \\ & \beta \text{KL} (p(z) \| p(z')) \end{aligned} \quad (1.15)$$

Finally, this method was tested in a variety of scenarios, including both single-object and multiple-object manipulation with different manipulation primitives (Figure 1.31). However, in the multi-object scenarios, the system was only tested on single-object manipulation primitives.

This work is particularly noteworthy as it demonstrates that a policy can be learned by solving an inverse problem, starting from

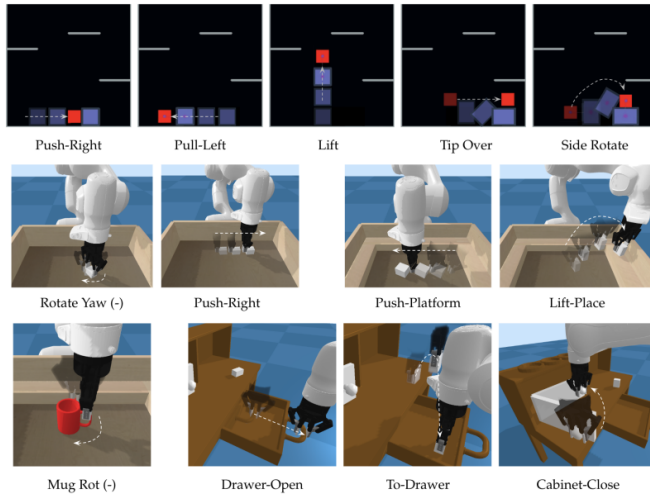


Figure 1.31: Testing scenarios and primitives proposed in [85]. (Top) **Block2D** Environment primitive examples. (Center) **Block3D** and **Block3DPlatform** primitive examples. (Bottom) The left image shows an example primitive in **Mug3D-Platforms**. The right three images show sample tasks from **Playroom3D**.

object affordances and deriving the corresponding robot trajectories. It also shows that the policy can be conditioned based on the desired goal state. However, certain aspects were not addressed in this work, such as the potential presence of distractor objects and tasks requiring the manipulation of multiple objects. Additionally, the affordances were learned in the object space (i.e., with known object poses) rather than in the high-level image space.

1.3.3.1.1 Discussion

1.3.3.2 Inverse Reinforcement Learning

The *Inverse Reinforcement Learning* (IRL) problem, also known as *Inverse Optimal Control*, is a LfD algorithm that addresses a significant challenge in Reinforcement Learning: designing an appropriate reward function for a given problem.

In many manipulation problems [89], using a binary and sparse reward function, where the reward is 1 if the task is completed correctly and 0 otherwise, can result in very long and inefficient training periods. For instance, in a reaching problem where the goal is to simply reach an object, the agent would receive a reward of 0 most of the time. More critically, actions that bring the agent closer to the object and actions that move it farther away would yield the same reward. In this simple example, a better reward function would measure the relative distance between the agent and the object. While this information can be easily obtained in simulations, it is often unavailable in real-world settings, forcing algorithm designers to make assumptions such as having prior knowledge about the object’s location.

To address this issue, several research approaches have been proposed. One prominent approach is *Reward Shaping*. In this method, the goal is to make the reward function more informative by introducing intermediate rewards during the agent’s experience. These intermediate rewards are hand-engineered and require some degree of *domain knowledge*.

The second approach, which is the focus of this chapter, is Inverse Reinforcement Learning (IRL). In IRL, the main idea is to **learn** the reward function R which explains the expert behaviors contained in the dataset \mathcal{D}^E , and then use the learned R to train the agent using classic RL algorithms.

The IRL procedure was introduced in [90], and it is described by Algorithm 4. Essentially, the IRL algorithm is an iterative process where the parametrized reward function R_ω is first updated according

to a given objective function \mathcal{L} . Subsequently, the updated reward function is used to update the learner's policy π_θ^L .

Algorithm 4 Classic feature matching IRL algorithm

Require: Dataset of expert trajectories $\mathcal{D}^E = \{\tau_i^E\}_{i=1}^N$
Require: Reward function R_ω , policy π_θ^L

while policy improves **do**

- Evaluate the state-action visitation frequency μ of the current policy π_θ^L
- Evaluate the objective function \mathcal{L} , w.r.t. μ and the dataset \mathcal{D}^E
- Update the reward-function parameters ω based on \mathcal{L}
- Update the policy π_θ^L through an RL algorithm, using the updated R_ω

end while

Generally speaking, the IRL approach faces two main challenges:

- The learning process can be time-consuming and impractical for high-dimensional problems due to the double-nested optimization procedure.
- The IRL problem is *ill-posed* because multiple reward functions can produce the same set of actions.

Despite these practical and theoretical challenges, various significant scientific contributions have been made in this field.

To solve the problem of multiple solutions for the reward function, constraints have been added to the optimization problem. Specifically, based on the type of constraint, there are two approaches:

- (a) The *Maximum Margin Prediction* (MMP) approach [91, 92].
- (b) The *Maximum Entropy* (Max-Ent) approach [93, 94, 95].

The *MMP* methods assume that the demonstrated trajectories are **optimal** and operate in a **deterministic** setting. The aim is to find the cost function such that the reward of the demonstrated trajectories, $R(\tau^E)$, is greater than the reward of all alternative trajectories, $R_\omega(\tau)$, by a certain margin m , solving the optimization problem formalized in Formula 1.16.

$$\max_{\omega, m} m \quad \text{s.t.} \quad R_\omega(\tau^E) \geq \max(R_\omega(\tau)) + m \quad (1.16)$$

The main problem with this formulation is that it does not handle the case in which the expert behavior is sub-optimal, leading to an ambiguous notion of margin.

In the *Max-Ent* approach, the goal is to find the reward function parameters ψ that drive the policy to maximize the entropy, subject to feature expectation matching (Formula 1.17).

$$\max_{\psi} \mathcal{H}(\pi^{r_\psi}) \quad \text{s.t.} \quad \mathbb{E}_{\pi^{r_\psi}}[\mathbf{f}] = \mathbb{E}_{\pi^*}[\mathbf{f}] \quad (1.17)$$

The Max-Ent approach is the most popular in the IRL field since it removes the ambiguous aspects of the previous formulation. In the original work, the reward function was a linear combination of the features, i.e., $r_\psi = \psi^T \mathbf{f}$. However, this reward formulation is not suited for high-dimensional feature spaces, which may require the capability to model non-linear reward structures. In [94], a deep neural network was used to model the reward function. In this work, the neural network maps the feature vector \mathbf{f} to the reward value and is trained according to the Maximum-Entropy setting. Experimental results have shown that the ability to approximate highly non-linear reward functions is essential for successfully solving tasks in high-dimensional discrete state spaces. A generalization to continuous state spaces was proposed in [95].

In particular, [95] addressed the problem of learning a cost function in a high-dimensional continuous state space with **unknown dynamics**. Starting from the exponential trajectory distribution $p(\tau) =$

$\frac{1}{Z} \exp(-c_\theta(\tau))$, the main difficulty is the estimation of the partition function Z , needed to compute the negative log-likelihood loss function (Formula 1.18).

$$\mathcal{L}_\theta = \frac{1}{N} \sum_{\tau_i^E \in D_{demo}} c_\theta(\tau_i^E) + \log(Z) \quad (1.18)$$

Since the dynamics are unknown, the idea was to estimate the partition function through the trajectories obtained from the current policy rollouts, with the hypothesis that, during the learning of the cost function, the current policy drives the distribution towards regions where samples are more useful.

Algorithm 5 Guided-Cost-Learning Algorithm [95]

Require: Initial controller $q_k(\tau)$

for $i = 1, \dots, N$ **do**

 Generate D_{traj} from $q_k(\tau)$

$\mathcal{D}_{samp} \leftarrow \mathcal{D}_{samp} \cup \mathcal{D}_{traj}$

 Update the cost-function parameters, using \mathcal{D}_{samp} and $\nabla_\theta \mathcal{L}(\theta)$

 Update the controller $q_{k+1}(\tau) \leftarrow q_k(\tau)$ according to [96] and using

\mathcal{D}_{traj}

end for

Starting from these considerations, Algorithm 5 was proposed. The algorithm returns a *Linear-Quadratic Gaussian* [96] controller q_k , obtained by solving the problem in Formula 1.19.

$$\begin{aligned} q_k &= \arg \min_q \mathbb{E}[c_\theta(\tau)] - \mathcal{H}(\tau) \\ \text{s.t. } p(s_{t+1}|s_t, a_t) &= \mathcal{N}(s_{t+1}; f_{x_t} x_t + f_{u_t} u_t, F_t) \end{aligned} \quad (1.19)$$

The cost function was parameterized according to a neural network, and experiments performed on real-robot manipulation tasks

such as dish placement and pouring proved the effectiveness of the proposed method and the necessity of a non-linear representation of the cost function for complex problems, outperforming the classic Max-Ent method.

Recent methods have aimed to advance IRL towards more complex learning scenarios, such as learning a reward function from video demonstrations. In [97], the architecture shown in Figure 1.32 was proposed. The goal was to obtain the parameters Ψ of a cost function $C_\Psi(\hat{\tau}, z_{goal})$, enabling the derivation of a sequence of actions by minimizing the cost function itself (Formula 1.20).

$$\mathbf{a}_{new} = \mathbf{a} - \eta \nabla_a C_\Psi(\hat{\tau}, z_{goal}). \quad (1.20)$$

Different cost functions were proposed, all aiming to reduce the distance between the current predicted keypoints and the goal keypoint configuration. The trajectory $\hat{\tau}$ is a sequence of predicted states $[\hat{s}_1, \dots, \hat{s}_T]$, resulting from a learned dynamic model, $\hat{s}_{t+1} = f_{dyn}(\hat{s}_t, a_t)$.

Experimental results demonstrated that it is possible to learn a cost function from human/robot video demonstrations. However, the proposed setting was tested on a very simple reaching task, highlighting that much work remains to be done to establish the effectiveness or ineffectiveness of IRL in complex real-robot manipulation tasks starting from video demonstrations.

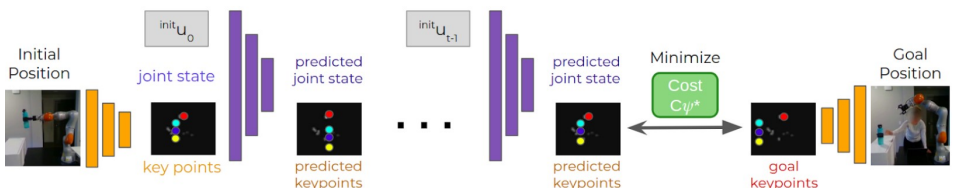


Figure 1.32: Architecture proposed in [97]

1.3.3.3 Generative Adversarial Imitation Learning

The *Generative Adversarial Imitation Learning* (GAIL) is a Learning from Demonstration (LfD) approach proposed by the authors of [98]. The rationale behind GAIL was to improve the Inverse Reinforcement Learning (IRL) setting, which is expensive to run due to the double-nested optimization procedure. To achieve this objective, the authors in [98] started from the Max-Ent formulation in Formula 1.21, and obtained a characterization of the learned policy. This characterization combines the learning of the reward function and the learning of the policy through a reinforcement learning algorithm. In Formula 1.21, $\psi(c)$ is a cost-regularizer, $\psi^*(c)$ is its conjugate, and ρ_π is the occupancy measure, i.e., the distribution of state-action pairs that the agent encounters when navigating the environment with policy π .

The next step was to choose an appropriate regularization function. In particular, by choosing the regularizer in Formula 1.23, the conjugate in Formula 1.24 can be obtained. This is the classic Adversarial Learning Loss, where the current policy π^L acts as the GAN generator, and D is the GAN discriminator, which must distinguish between state-action pairs generated either by the expert policy or by the current policy.

$$\begin{aligned} IRL_\psi(\pi^E) = \arg \max_{c \in \mathbb{R}^{S \times A}} & -\psi(c) + \\ & \left(\min_{\pi^L \in \Pi} -\mathcal{H}(\pi^L) + \mathbb{E}_{\pi^L} [c(s, a)] \right) - \\ & \mathbb{E}_{\pi^E} [c(s, a)] \end{aligned} \quad (1.21)$$

$$RL \circ IRL_\psi(\pi^E) = \arg \min_{\pi^L \in \Pi} -\mathcal{H}(\pi^L) + \psi^*(\rho_{\pi^L} - \rho_{\pi^E}) \quad (1.22)$$

$$\begin{aligned}\psi_{GA}(c) &= \begin{cases} \mathbb{E}_{\pi^E} [g(c(s, a))] & \text{if } c < 0 \\ +\infty & \text{otherwise} \end{cases}, \\ g(x) &= \begin{cases} -x - \log(1 - e^x) & \text{if } c < 0 \\ +\infty & \text{otherwise} \end{cases}\end{aligned}\tag{1.23}$$

$$\begin{aligned}\psi_{GA}^*(\rho_{\pi^L} - \rho_{\pi^E}) &= \max_{D \in (0,1)^{S \times A}} \mathbb{E}_{\pi^L} [\log(D(s, a))] + \\ &\quad \mathbb{E}_{\pi^E} [\log(1 - D(s, a))]\end{aligned}\tag{1.24}$$

Based on these considerations, Algorithm 6 has been proposed. Specifically, the GAIL algorithm is an iterative procedure composed of two main steps. The first step involves updating the discriminator D , which must distinguish between trajectories produced by the learned policy τ_i^L and trajectories produced by the expert τ^E . The second step involves updating the learner policy π^L according to some reinforcement learning algorithm (e.g., TRPO was used in [98]). The policy is updated in such a way that the trajectories it generates become indistinguishable from those of the expert for the discriminator, i.e., the learner produces state transitions that are similar to those of the expert.

In the seminal work [98], GAIL has proven to be more effective than classic IRL (Inverse Reinforcement Learning) algorithms [93, 100]. The authors evaluated the GAIL algorithm on nine classic simulated control tasks from the OpenAI Gym simulator [101]: Cartpole, Acrobot, MountainCar, HalfCheetah, Hopper, Walker, Ant, Humanoid, and Reacher.

The observation and control spaces for these tasks are detailed in Table 1.6, and the performance results are shown in Figure 1.33. From these results, it is evident that the GAIL algorithm overcomes classic

Algorithm 6 Generative Adversarial Imitation Learning Algorithm

Require: Expert Trajectories $\tau^E \sim \pi^E$, initial policy π_θ^L , discriminator D_ω

for $i = 1, \dots, N$ **do**

 Sample trajectories, $\tau_i^L \sim \pi_\theta^L$

 Update Discriminator, with the gradient

$$\hat{\mathbb{E}}_{\tau_i^L} [\nabla_\omega \log(D_\omega(s, a))] + \hat{\mathbb{E}}_{\tau^E} [\nabla_\omega \log(1 - D_\omega(s, a))]$$

 Update Policy π_θ^L , with TRPO [99], using the cost-function $C(s, a) = \log(D_\omega(s, a))$, and the KL-constrained gradient step

$$\hat{\mathbb{E}}_{\tau_i} [\nabla_\theta \log \pi_\theta(a | s) Q(s, a)] - \lambda \nabla_\theta H(\pi_\theta)$$

$$Q(\bar{s}, \bar{a}) = \hat{\mathbb{E}}_{\tau_i} [\log(D_\omega(s, a)) \mid s_0 = \bar{s}, a_0 = \bar{a}]$$

end for

IRL algorithms in terms of both pure reward and sample efficiency. Consequently, subsequent research has focused on improving the algorithm's efficiency in terms of environment interaction. This has been achieved by replacing the model-free, on-policy TRPO algorithm with an off-policy RL algorithm, as seen in [102], or by modifying the reward function input to the RL algorithm [103, 104].

However, as noted in Table 1.6, the tested tasks are characterized by low-dimensional state spaces. More recent research [105, 106, 107, 108] has focused on testing the GAIL algorithms in high-dimensional state spaces, where the input is an image. Specifically, with respect to the Adversarial Imitation Learning setting, works of interest are [107, 108].

In [107], the authors focused on solving the **casual-confusion** problem. This problem occurs when the discriminator, during the learning process, focuses on task-irrelevant features between expert

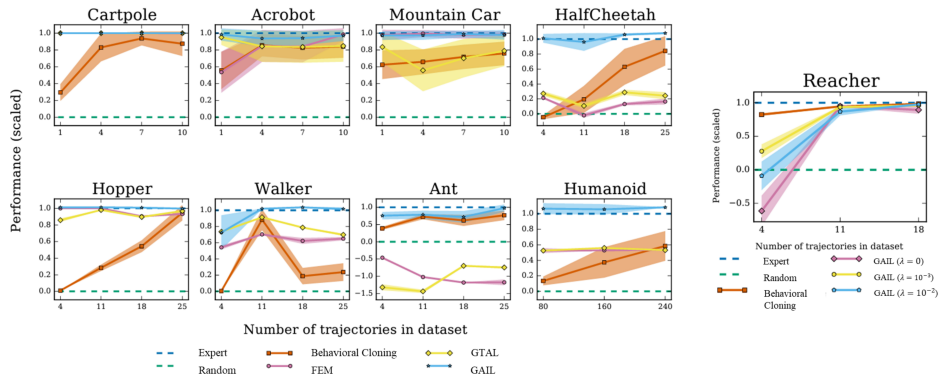


Figure 1.33: The performance comparison proposed in [98] is presented here. The y-axis shows the scaled reward, where the expert’s reward is set to 1 and the random baseline is set to 0. The IRL baselines FEM and GTAL refer to the IRL algorithm described in [100], but with different cost functions.

and policy generated transitions, for example a difference in the expert and agent embodiment like the gripper, this causes the rewards to become uninformative. To reduce the casual-confusion problem, in [107] two elements have been proposed:

1. A *regularization term*, with the aim to make the discriminator **unable** to distinguish between constraining sets I_E and I_A . These sets are composed of expert and agent observations, such that a sample can belong either to I_E or I_A , based on spurious features (e.g., a different gripper color);
2. An *early-stopping policy* called Actor Early-Stopping (AES), that restarts the episode if the discriminator score at the current step exceeds the median score of the episode so far for T_{patience} consecutive steps.

Table 1.6: Observation and Action space for the tasks used in [98]

Task	Observation space	Action space
Cartpole	4 (continuous)	2 (discrete)
Acrobot	4 (continuous)	3 (discrete)
Mountain Car	2 (continuous)	3 (discrete)
Reacher	11 (continuous)	2 (continuous)
HalfCheetah	17 (continuous)	6 (continuous)
Hopper	11 (continuous)	3 (continuous)
Walker	17 (continuous)	6 (continuous)
Ant	111 (continuous)	8 (continuous)
Humanoid	376 (continuous)	17 (continuous)

To prevent the discriminator from focusing on task-irrelevant features, the authors proposed a regularization term based on the constraining-set accuracy defined in Formula 1.25. The idea is that if the discriminator achieves an accuracy greater than $\frac{1}{2}$ on the constraining set, the maximized adversarial cost function should be inverted, as shown in Formula 1.26.

$$\text{accuracy}(I_E, I_A) = \frac{1}{2} \mathbb{E}_{s \in I_E} [\mathbf{1}_{D_\omega \geq \frac{1}{2}}] + \frac{1}{2} \mathbb{E}_{s \in I_A} [\mathbf{1}_{D_\omega < \frac{1}{2}}] \quad (1.25)$$

$$\begin{aligned} \mathcal{L}_\psi(s_E, s_A, \hat{s}_E, \hat{s}_A) &= G_\psi(s_E, s_A) \\ &\quad - \mathbf{1}_{\text{accuracy}(\hat{s}_E, \hat{s}_A) \geq \frac{1}{2}} G_\psi(\hat{s}_E, \hat{s}_A), \end{aligned}$$

$$\begin{aligned} \text{where } G_\psi(s_E, s_A) &= \sum_{i=1}^N \log D_\psi(s_E^{(i)}) \\ &\quad + \log [1 - D_\psi(s_A^{(i)})] \end{aligned} \quad (1.26)$$

The proposed system was tested on 4 tasks (Figure 1.34), with the

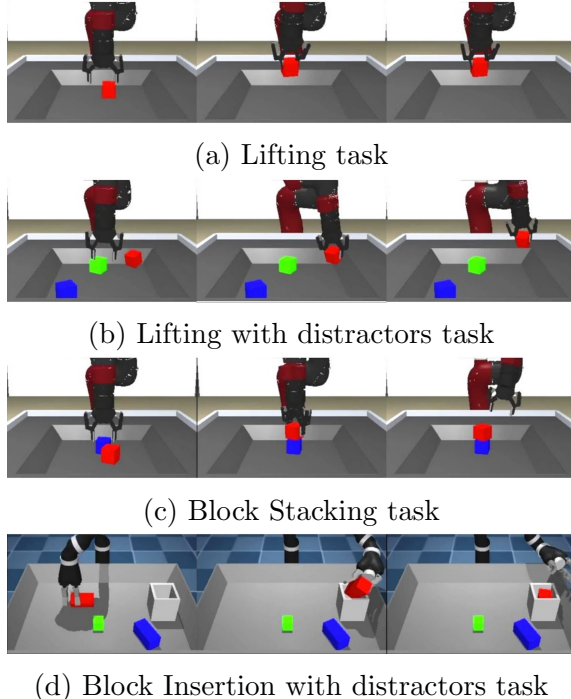


Figure 1.34: Tasks solved in [107]

agent trained on each single task, according to the *Distributed Distributional Deterministic Policy Gradients* (D4PG) [109] RL algorithm, with reward-function $R(s_t) = -\log(1 - D_\omega(s_t))$. Experimental results have shown how the proposed system overcomes the GAIL [98] baseline, both in setting with spurious features and without spurious features (Figure 1.35).

The authors of [108] proposed a more data-efficient Adversarial Imitation Learning method. They leveraged a model-based approach within a high-dimensional state space. Instead of generating a dynamic model in the image space, i.e., training a generative model to

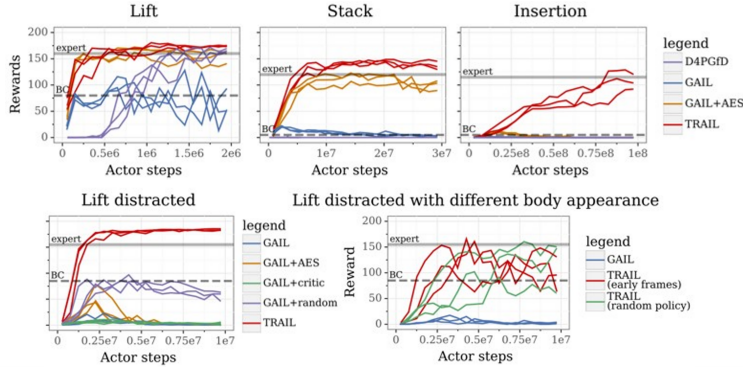


Figure 1.35: Experimental results on tasks without and with spurious features [107]

produce the next image based on the current image and the performed action. Their method encodes observations defined in the image space into a corresponding latent space characterized by vectors of smaller dimensions. Then, they learn a dynamic model in that space, training a generative model to produce the next embedding based on the current encoded observation and the performed action. The proposed learning procedure is based on three main steps:

1. Learn the *Latent Dynamic Model*, $(\hat{\mathcal{U}}_\beta, \hat{\mathcal{T}}_\beta, q_{beta})$, by maximizing the Evidence Lower Bound (Formula 1.27), where $\hat{\mathcal{U}}_\beta$ is the decoder, q_{beta} is the encoder, and $\hat{\mathcal{T}}_\beta$ is the transition model;
2. Train a *discriminator*, D_θ , by minimizing the Adversarial Loss function (Formula 1.28);
3. Train a *policy* π_θ^L , by maximizing the Value function (Formula 1.29).

$$\begin{aligned} \max_{\beta} \mathbb{E}_{q_{\beta}} & \left[\sum_t \log(\hat{\mathcal{U}}_{\beta}(s_t | z_t)) \right. \\ & \left. + \mathbb{D}_{KL}(q_{\beta}(z_t | s_t, z_{t-1}, a_{t-1}) || \hat{\mathcal{T}}_{\beta}(z_t | z_{t-1}, a_{t-1})) \right] \end{aligned} \quad (1.27)$$

$$\begin{aligned} \min_{\theta} \mathbb{E}_{(z,a) \sim \rho^E(z,a)} & [-\log(D_{\theta}(z, a))] \\ & + \mathbb{E}_{(z,a) \sim \rho_{\hat{\mathcal{T}}}^{\pi^L}} [-\log(1 - D_{\theta}(z, a))] \end{aligned} \quad (1.28)$$

$$\begin{aligned} \max_{\pi_{\theta}^L} V_{\theta,\beta}^K(z_t) = \max_{\pi_{\theta}^L} \mathbb{E}_{\pi_{\theta}^L, \hat{\mathcal{T}}_{\beta}} & \left[\sum_{\tau=t}^{t+K-1} \gamma^{\tau-t} \log(D_{\theta}(z_{\tau}^{\pi_{\theta}^L}, a_{\tau}^{\pi_{\theta}^L})) \right. \\ & \left. + \gamma^K V_{\beta}(z_{t+K}^{\pi_{\theta}^L}) \right] \end{aligned} \quad (1.29)$$

With this learning setting the proposed system outperforms previous works such as [106, 102] both in terms of **data-efficiency** and **overall performance**, on a set of continuous control tasks.

Generally speaking, the Generative Adversarial Imitation Learning has shown very promising performance in simulated control tasks and simulated robot manipulation tasks, even in complex high-dimensional state-space. However, it is not so clear, how these methods could perform in real-world robotic manipulation tasks, in terms of data-efficiency, generalization capability, and safety during real-world interactions.

1.3.3.4 Learning from Observation

In all the previous sections, the methodologies assume access to the agent actions, working with state-action trajectories. In *Learning from*

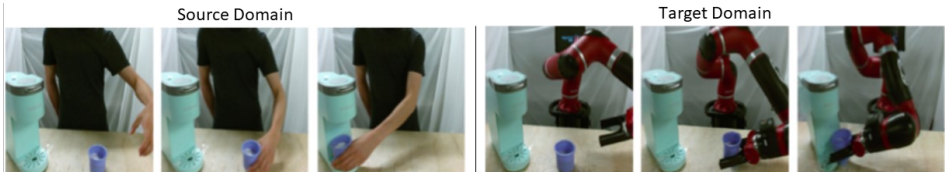


Figure 1.36: Representation of **embodiment mismatch problem**. (Left) The source domain represented by a video of human performing a task. (Right) The target domain, represented by the robot that executes the observed task

Observation (LfO), this assumption is relaxed, and methods for learning from **state-only** demonstrations are proposed. This approach has gained attention in recent years [34] because it theoretically allows a robotic system to be programmed as naturally as possible. Ideally, a robotic system should be able to reproduce a task by observing a human or another robot performing it, without access to the actions performed, unlike the methods described so far.

To address this problem, several questions need to be answered:

1. How can embodiment mismatches be resolved when the demonstrator has a different embodiment than the imitator?
2. How can the correspondence problem be handled when the demonstrator viewpoint differs from the imitator?
3. Once the perception subsystem issues are resolved, how is the policy π^L obtained?

The first question refers to the *correspondence problem* introduced in Section 1.3.2. This problem arises when the demonstrator embodiment differs from that of the learner, meaning that methods cannot directly use the recorded trajectories of the demonstrator.

One approach to solving this problem is to use methods that perform *image-to-image* translation. This involves using generative deep architectures to transform images of a subject in one domain (e.g., a human demonstrator) into images where the context remains the same, but the subject is different (e.g., the human demonstrator is replaced by the target robot) as depicted in Figure 1.36. This approach has been followed by authors in [31, 35, 110].

Specifically, the authors in [31, 35] used the Cycle-GAN architecture [111] to translate images from the source domain (human images) to the target domain (robot images) in an unsupervised manner. The work in [111] shifted the translation problem from a paired image setting, where each source domain image has a corresponding target domain image, to an unpaired image setting, where the source domain image does not have a corresponding target domain image.

To address this, Cycle-GAN introduces a novel learning procedure involving two translation models: $G : X \rightarrow Y$ and $F : Y \rightarrow X$. The first model maps inputs from the source domain to the target domain, while the second model maps inputs from the target domain back to the source domain. These two models are trained in an adversarial setting by minimizing the loss function shown in Formula 1.30.

$$\begin{aligned}\mathcal{L}(G, F, D_X, D_Y) = & \mathcal{L}_{GAN}(G, D_Y, X, Y) + \\ & \mathcal{L}_{GAN}(F, D_X, Y, X) + \lambda \mathcal{L}_{cyc}(G, F)\end{aligned}$$

$$\begin{aligned}\mathcal{L}_{GAN}(Z, D_K, S, T) = & \mathbb{E}_{t \sim p_{data}(t)} [\log(D_K(t))] + \\ & \mathbb{E}_{s \sim p_{data}(s)} [\log(1 - D_K(Z(s)))]\end{aligned}\tag{1.30}$$

$$\begin{aligned}\mathcal{L}_{cyc}(G, F) = & \mathbb{E}_{x \sim p_{data}(x)} [\|F(G(x)) - x\|_1] + \\ & \mathbb{E}_{y \sim p_{data}(y)} [\|G(F(y)) - y\|_1]\end{aligned}$$

Here, \mathcal{L}_{GAN} is the adversarial loss component, where the discriminator

D_K is trained to distinguish between real samples $t \in T$ and translated samples $Z(s)$. The generator Z is trained to generate samples that are as similar as possible to those in the target domain, starting from samples in the source domain. Meanwhile, \mathcal{L}_{cyc} is a loss term that aims to maintain consistency between the generated samples and the ground truth one.

The application of this concept in the domain of interest, lead to a dataset for the source domain was composed of human demonstrations as well as a small amount of “random” data, in which the human moves around the scene but does not specifically attempt the task, while for the target domain, it consists of robot images executing randomly sampled actions in a few different settings.

The second question also addresses a variant of the correspondence problem, where, in addition to the embodiment mismatch, the problem of *different viewpoints* is also encountered (Figure 1.37a). This issue has been tackled in [112, 105].

In [112], a Convolutional Neural Network was trained using a *Triplet-Loss* [113]. The aim was to train a network to predict an embedding independent of the viewpoint, but containing only task-relevant features. To achieve this, the network had to produce an embedding, $f(x)$, such that $\|f(x_i^a) - f(x_i^p)\|_2^2 + \alpha < \|f(x_i^a) - f(x_i^n)\|_2^2$ for all $(f(x_i^a), f(x_i^p), f(x_i^n)) \in \mathcal{T}$, where \mathcal{T} is the set of all possible triplets in the dataset. This implies that embeddings produced by samples from different viewpoints, but sharing the same time-step, (x_i^a, x_i^p) , should be similar, while embeddings produced by samples from the same viewpoint, but at different time-steps, (x_i^a, x_i^n) , should be different (Figure 1.37a).

In [105], a different approach was employed. Here, a *context translation problem* was addressed using an Encoder-Decoder architecture (Figure 1.37b). The proposed architecture was trained on pairs of demonstrations, $\mathcal{D}_i = [o_0^i, o_1^i, \dots, o_T^i]$ and $\mathcal{D}_j = [o_0^j, o_1^j, \dots, o_T^j]$, composed of visual observations. Samples in \mathcal{D}_i come from the source

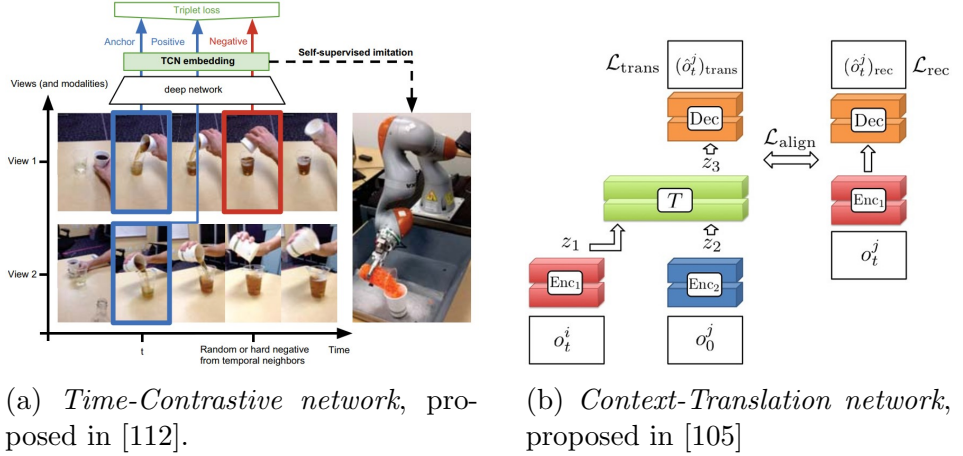


Figure 1.37: Examples of how the mismatch between demonstrator viewpoint and learner viewpoint can be handled.

context ω_i , while samples in \mathcal{D}_j come from the target context ω_j . The model must output the observations in \mathcal{D}_j conditioned on both \mathcal{D}_i and the first observation o_0^j from the target domain.

As will be explained next, the outputs of both the Time-Contrastive and the Context-Translation networks can be used to obtain an engineered reward function.

The third question concerns the method by which the final learned policy is derived. To present the different approaches, it is essential to distinguish between *Model-Free* and *Model-Based* methods (Figure 1.38).

Model-Free

Model-Free methods are characterized by the fact that they do not leverage knowledge about the environment dynamics, which can either be given a priori or learned through data-driven approaches. A further classification must be done between *Reward Engineering* and

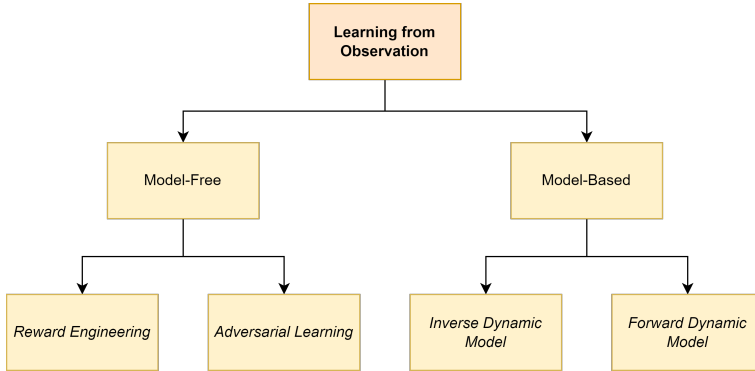


Figure 1.38: Learning from Observation taxonomy

Adversarial Learning approaches.

Reward Engineering methods are characterized by the use of a hand-designed reward function to train the policy according to the Reinforcement Learning paradigm [2]. Methods based on this approach include [105, 112, 35, 114].

In [105], the reward function is defined as in Formula 1.31.

$$\begin{aligned}
 R(o_t^l) = & - \left\| Enc_1(o_t^l) - \frac{1}{n} \sum_{i=1}^n F(o_t^i, o_0^l) \right\|_2^2 - \\
 & w_{rec} \left\| o_t^l - \frac{1}{n} \sum_{i=1}^n M(o_t^i, o_0^l) \right\|_2^2
 \end{aligned} \tag{1.31}$$

The first term is the classic Feature Tracking reward function, which aims to minimize the Euclidean Distance between the encoding of the current learner observation o_t^l and the encoding of the demonstration in the learner context. The second term penalizes the policy for experiencing observations that differ from the translated observation.

In [112], the reward function is defined according to Formula 1.32.

$$R(\mathbf{v}_t, \mathbf{w}_t) = -\alpha \|\mathbf{w}_t - \mathbf{v}_t\|_2^2 - \beta \sqrt{\gamma + \|\mathbf{w}_t - \mathbf{v}_t\|_2^2} \quad (1.32)$$

Where \mathbf{v}_t is the TCN embedding of the video demonstration at timestep t , and \mathbf{w}_t is the TCN embedding produced by the robot observation (Figure 1.37a).

In [35], a **keypoint-representation** (Figure 1.39) is obtained for both the current robot observations z_t and each frame of the translated demonstration video $\{z_p^E\}_{p=1}^T$. The reward is then computed as in Formula 1.33.

$$\begin{aligned} R(z_t, z_{t+1}, z^E) = & -\lambda_1 \min_p \|z_t - z_p^E\| - \\ & \lambda_2 \min_p \|(z_{t+1} - z_t) - (z_{p+1}^E - z_p^E)\| \end{aligned} \quad (1.33)$$

The main idea is to generate actions that minimize the distance between the translated keypoints and the keypoints obtained from the current robot observation, thereby reproducing the demonstrated trajectory. The *min* operator is necessary because the robot and the demonstration are not temporally aligned; there is no a priori knowledge about which demonstration frame corresponds to the current agent state.

In [114], the reward function was defined as $R(s_t) = -\frac{1}{k} \|\phi(s_t) - g\|_2^2$, where g is the goal embedding, defined as the mean embedding of the last frame of all the demonstration videos in the dataset, while $\phi(s_t)$ is the embedding of the current observation. Experimental results, on simulation data proved that the proposed method can be used to learn tasks from cross-embodiment demonstrations, outperforming baseline [112] in terms of both sample efficiency and performance.

Adversarial Learning methods rely on the Adversarial Learning paradigm and are closely related to the GAIL methods (Section 1.3.3.3).

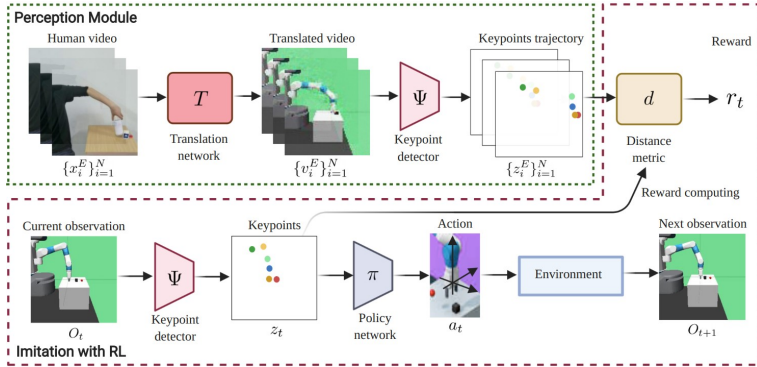


Figure 1.39: Architecture proposed by [35]

Unlike the methods discussed in the GAIL section, these methods do not assume access to the demonstrator’s actions. Preliminary works in this area have been proposed in [115, 116].

The goal of authors in [115] was to demonstrate that the Adversarial Learning setting can be effectively used even without action information. To test this hypothesis, the authors conducted a series of experiments in simulation for a walking task, where the same RL policy was trained in two contexts: one where the Discriminator had access to the (state, action) pair, and another where the Discriminator had access to state-only demonstrations. The results showed no substantial difference between the two settings, supporting the hypothesis that the essential information for task learning is contained in the state.

The next significant work was proposed by the authors of [116], who formalized the *GAIIfO* algorithm (Algorithm 7), an extension of GAIL [98] to state-only demonstrations. The proposed algorithm was used to train a network to solve tasks in a simulation environment [101], with both low-dimensional state representation and visual-state representation. Results regarding the number of demonstrated trajec-

Algorithm 7 GAIIfO algorithm [116]

Require: Initial policy π_ϕ^L , Initial Discriminator D_θ

Require: State-only expert demonstration trajectories $\tau^E = \{(s, s')\}$

while Policy Improves **do**

 Execute π_ϕ^L and collect state transitions $\tau^L = \{(s, s')\}$

 Update D_θ , with $\mathcal{L}_{D_\theta} = -(\mathbb{E}_{\tau^L}[\log(D_\theta(s, s'))] + \mathbb{E}_{\tau^E}[\log(1 - D_\theta(s, s'))])$

 Update π_ϕ^L , with reward $r_{\pi_\phi^L} = -(\mathbb{E}_{\tau^L}[\log(D_\theta(s, s'))])$

end while

tories are reported in Figure 1.40.

As noted from the results, GAIIfO outperforms previous observation-based methods [112, 117] in settings with a low number of expert trajectories. The main drawback of GAIIfO is the **high number of environmental interactions** needed to learn a policy, as it uses the model-free TRPO [99] algorithm. This issue was addressed by DEALIO [118], which replaced the model-free algorithm with PILQR [119], a model-based RL algorithm discussed next.

Model-Based

Model-Based methods leverage knowledge about the environment dynamics, which is learned through data-driven approaches. These methods can be further classified into *Inverse Dynamic Model* and *Forward Dynamic Model* approaches.

The *Inverse Dynamic Model* approach, given a transition (s_t, s_{t+1}) , obtains a function M that maps state transitions to actions, i.e., $a_t = M(s_t, s_{t+1})$. In contrast, the *Forward Dynamic Model* approach, given a state-action pair (s_t, a_t) , aims to learn a function F that generates the next state s_{t+1} , i.e., $s_{t+1} = F(s_t, a_t)$.

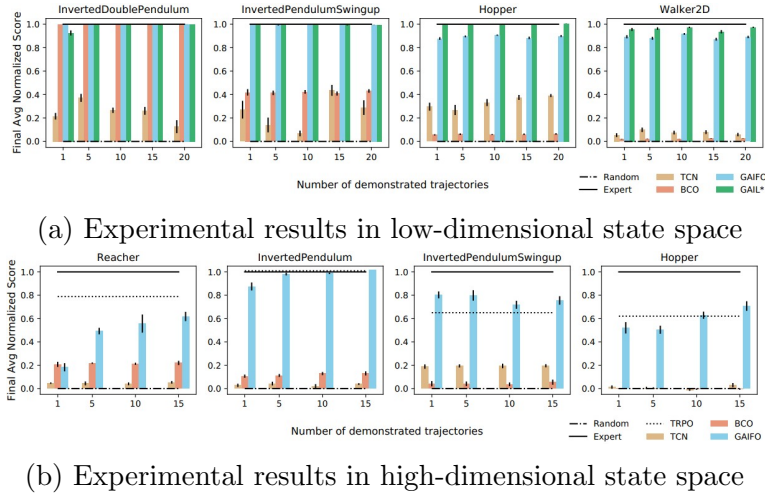


Figure 1.40: Experimental results reported in [116].

Inverse Dynamic Model methods include [120, 117, 121, 122].

In [120], the goal was to develop a system capable of tying a knot in a rope. A self-supervised learning approach was used to train a Convolutional Neural Network. Given a pair of images (I_t, I_{t+1}) representing two successive rope states, the network was able to determine the action required to transition from state I_t to state I_{t+1} . The network was trained using a dataset of 30K tuples (I_t, a_t, I_{t+1}) collected via an exploratory policy.

Authors in [117] proposed a general approach, depicted in Figure 1.41, composed of two main parts: the learned Inverse Dynamic Model, M_θ , and the learned policy π_ϕ . The learning procedure is iterative. The model M_θ^i is updated by maximizing the probability $p_\theta(a_t|s_t, s_{t+1})$, using tuples (s_t, a_t, s_{t+1}) collected by the current policy. Once the dynamic model is updated, it infers the action \tilde{a}_t given the demonstrations. The policy, having access to both state and action information, is then trained using classic Behavioral Cloning (BC) by

optimizing the policy parameters through maximum-likelihood estimation $\phi^* = \underset{\phi}{\operatorname{argmax}} \prod_{i=0}^N \pi_{\phi}^L(\tilde{a}_i | s_i)$.

In [121], a similar approach to [117] was used, but the agent's policy was trained using a combination of Behavioral Cloning and the Advantage Actor Critic (A2C) objective function [123] (Formula 1.34).

$$\mathcal{L}_{\theta}^{hyb} = \mathbb{E}_{s,a} [A(s) \log(a|s; \theta) + \alpha \mathcal{H}(\pi^L(.|s))] + \mathbb{E}_{(\hat{s}_t, \hat{s}_{t+1}) \sim D} [\log(\pi^L(M(\hat{s}_t, \hat{s}_{t+1})|\theta))]. \quad (1.34)$$

The main drawback is the assumption of access to the reward function, which can limit its applicability in real-robot manipulation tasks.

In [122], the work in [124] was extended to state-only demonstrations, and the *State-Only Imitation Learning* (SOIL) algorithm was proposed. This method addresses complex dexterous manipulation tasks, such as object reallocation, tool use, in-hand manipulation, and door opening, using a simulated humanoid hand. A neural network representing the Inverse Dynamic Model was trained by minimizing the L2-loss, given the action performed during the policy rollout. The policy was then updated according to the *Demo Augmented Policy Gradient* (DAPG) method [124], adapted for state-only demonstrations, which follows the gradient updates described by Formula 1.35.

$$g_{SOIL} = g + \lambda_0 \lambda_1^k \sum_{(s_t, \tilde{a}_t) \in D'} \nabla_{\theta} \log \pi_{\theta}^L(\tilde{a}_t, s_t), \quad (1.35)$$

where g is the Natural Policy Gradient term. The idea is to leverage the demonstrations at the beginning of the training and then exploit the RL algorithm to improve the behavior. Experiments performed in simulation showed that, compared to pure RL, the proposed method converges faster and produces more human-like behaviors.

Forward Dynamic Model methods include [31, 118].

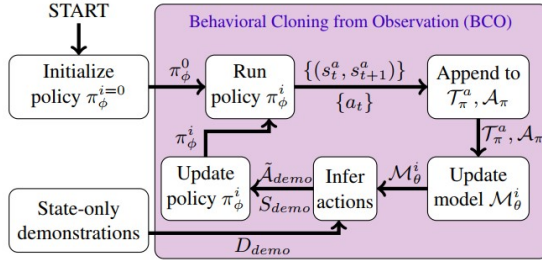


Figure 1.41: Representation of the learning procedure proposed by [117]

In [31], once the human video demonstration was translated into the corresponding robot video, the policy was learned using the model-based RL algorithm SOLARIS [125]. This algorithm optimizes a controller using the Linear-Quadratic Regulator (LQR) procedure. The policy optimization occurs in a low-dimensional, highly regularized *latent space*, generated using Variational Inference [126]. Starting from a sequence of observations and actions, a Global Dynamic Model over the latent trajectory is obtained. Then, given the Latent Dynamic Model, a Linear-Gaussian Controller is derived using LQR-FLM [96]. Real-world robotic experiments demonstrated that with just **2 hours** of robot interaction, it was possible to outperform previous works such as [112, 117] and classic BC algorithms in tasks like "coffee making" (Figure 1.36) and cup-retrieving, where the robot retrieves a cup from a closed drawer.

In [118], the sample inefficiency problem of GAIIfO [116] was addressed. The approach combined the adversarial learning setting with state-only demonstrations, which had shown promising results (Figure 1.40), with a more data-efficient RL algorithm like PILQR [119]. PILQR's core is the LQR optimization procedure. Generally, it returns a *linear-gaussian controller* (Formula 1.36) that optimizes a

quadratic-cost function (Formula 1.37) under the assumption of *linear-gaussian dynamics* (Formula 1.38).

$$\pi(a_t|s_t) = \mathcal{N}(K_t s_t + k_t, S_t) \quad (1.36)$$

$$c(s_t, a_t) = \begin{bmatrix} s_t \\ a_t \end{bmatrix}^T C_t \begin{bmatrix} s_t \\ a_t \end{bmatrix} + \begin{bmatrix} s_t \\ a_t \end{bmatrix}^T c_t + c_{ct} \quad (1.37)$$

$$s_{t+1} \sim P(s_{t+1}|s_t, a_t) = \mathcal{N}(F_t \begin{bmatrix} s_t \\ a_t \end{bmatrix} + f_t, \Sigma_t) \quad (1.38)$$

To use this framework, the linear-gaussian dynamic model was fitted using the current policy rollouts. Then, to obtain a quadratic cost function as needed by LQR, the dynamic model was used to express the modified discriminator output (Formula 1.39) as a function of the pair (s_t, a_t) .

$$D_\theta(s_t, s_{t+1}) = \frac{1}{2} \begin{bmatrix} s_t \\ s_{t+1} \end{bmatrix}^T C^{ss}(s_t, s_{t+1}) \begin{bmatrix} s_t \\ s_{t+1} \end{bmatrix} + \begin{bmatrix} s_t \\ s_{t+1} \end{bmatrix}^T c^{ss}(s_t, s_{t+1}) \quad (1.39)$$

Experiments performed in simulation with low-dimensional state spaces showed promising results (Figure 1.42b) in terms of sample efficiency compared to the GAIfO baseline. However, improvements are needed to: **(1)** Reduce variance to make the learning process more reliable, **(2)** Increase overall performance, **(3)** Adapt the algorithm for real-world robot manipulation tasks.

Generally, LfO methods have demonstrated interesting features, such as generating a policy from state-based information alone. This supports the hypothesis that the primary source of information for task learning is the sequence of state transitions. Extrapolating the valuable information to perform actions that induce the desired behavior may not be trivial, especially if the state space is represented

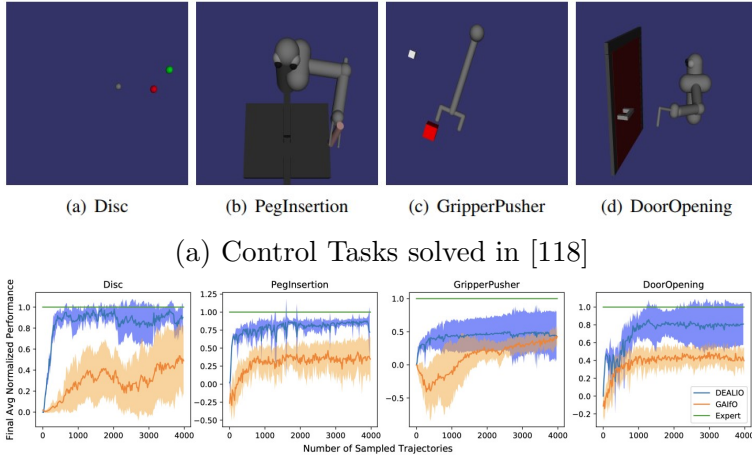


Figure 1.42: DEALIO: (1.42a) Control Tasks, (1.42b) Performance Level

by images of a human operator. This complexity leads to the design of architectures composed of different stages, which not only increase the complexity of the system itself but also the amount and diversity of data required for their training. Furthermore, many methods of interest have been tested in simulated or relatively simple scenarios, still leaving open whether these methods can be used in real-world complex robotic manipulation tasks.

1.3.4 Graph Neural Network for planning systems

Chapter 2

Conditioned object detector

In this chapter the COD is going to be described. Specifically, Section 2.1 will outline the detection problem being addressed. Section 2.2 will detail the proposed architecture designed to solve the described problem. Section 2.3 will discuss the experimental setup and present the results obtained from testing the proposed architecture.

2.1 Problem formulation

2.2 Architecture

2.3 Experiments

In this section, the performed experiments are going to be described. Specifically, in Section 2.3.1 the dataset used for training procedure will be described. Section 2.3.2 will report the obtained results.

2.3.1 Dataset

2.3.2 Results

This section presents the obtained results, divided into two main blocks. The first block (Section 2.3.2.1) discusses the results of the method trained to detect only the target object. The second block (Section 2.3.2.1) covers the results of the method trained to detect both the target object and the final (placing) location. For each method, results are reported for two different scenarios: first, where the method is trained in a single-task multi-variation scenario; and second, where the method is trained in a multi-task multi-variation scenario.

2.3.2.1 Target object detector

Single-task multi-variation scenario

Multi-task multi-variation scenario

2.3.2.2 Target object and final position detector

Single-task multi-variation scenario

Multi-task multi-variation scenario

Chapter 3

Object conditioned control policy

In this chapter the OCCP is going to be described. Specifically, Section 3.1 will outline the problem being addressed. Section 3.2 will detail the proposed architecture designed to solve the described problem. Section 3.3 will discuss the experimental setup and present the results obtained from testing the proposed architecture.

3.1 Problem formulation

3.2 Architecture

This section describes the entire policy architecture, specifically focusing on how the COD (Chapter 2) is integrated. There are two control architectures, differing in how the final control module predicts actions. Section 3.2.1 details the architecture that uses a single control module to predict actions for both the reaching and placing phases. In contrast, Section 3.2.2 describes the architecture that divides the con-

trol module into two distinct parts: one for computing actions during the reaching phase, and another for the placing phase.

3.2.1 Single control module

3.2.2 Double control modules

3.3 Experimental results

In this section, the performed experiments are going to be described. Specifically, in Section 3.3.1 the dataset used for training procedure will be described. Section 3.3.2 will report the obtained results.

3.3.1 Dataset

3.3.2 Results

This section presents the obtained results, divided into two main blocks. The first block (Section 3.3.2.1) discusses the results of the method described in Section 3.2.1. The second block (Section 3.3.2.2) covers the results of the method described in 3.2.2. For each method, results are reported for two different scenarios: first, where the method is trained in a single-task multi-variation scenario; and second, where the method is trained in a multi-task multi-variation scenario.

3.3.2.1 Single control module

Single-task multi-variation scenario

Multi-task multi-variation scenario

3.3.2.2 Double control modules

Single-task multi-variation scenario

Multi-task multi-variation scenario

Chapter 4

Graph Neural Network for heuristic estimation

Chapter 5

Real world application

This chapter details the validation of the proposed methods in a real world scenario. Specifically, Section 5.1 describes the experimental setup. Section 5.2 discusses the dataset used to train the system. Finally, Section 5.3 presents the results obtained.

5.1 Experimental Setting

5.2 Dataset

5.3 Results

Chapter 6

Conclusions

Bibliography

- [1] S. Bini, G. Percannella, A. Saggesse, and M. Vento, “A multi-task network for speaker and command recognition in industrial environments,” *Pattern Recognition Letters*, vol. 176, pp. 62–68, 2023.
- [2] R. S. Sutton and A. G. Barto, *Reinforcement learning: An introduction*. MIT press, 2018.
- [3] T. Osa, J. Pajarinen, G. Neumann, J. A. Bagnell, P. Abbeel, J. Peters *et al.*, “An algorithmic perspective on imitation learning,” *Foundations and Trends® in Robotics*, vol. 7, no. 1-2, pp. 1–179, 2018.
- [4] T. Zhang, Z. McCarthy, O. Jow, D. Lee, X. Chen, K. Goldberg, and P. Abbeel, “Deep imitation learning for complex manipulation tasks from virtual reality teleoperation,” in *2018 IEEE International Conference on Robotics and Automation (ICRA)*. IEEE, 2018, pp. 5628–5635.
- [5] A. Mandlekar, D. Xu, J. Wong, S. Nasiriany, C. Wang, R. Kulakarni, L. Fei-Fei, S. Savarese, Y. Zhu, and R. Martín-Martín, “What matters in learning from offline human demonstrations for robot manipulation,” in *Conference on Robot Learning*. PMLR, 2022, pp. 1678–1690.
- [6] S. Dasari and A. Gupta, “Transformers for one-shot visual imitation,” in *Conference on Robot Learning*. PMLR, 2021, pp. 2071–2084.

- [7] A. Brohan, N. Brown, J. Carbajal, Y. Chebotar, J. Dabis, C. Finn, K. Gopalakrishnan, K. Hausman, A. Herzog, J. Hsu, J. Ibarz, B. Ichter, A. Irpan, T. Jackson, S. Jesmonth, N. J. Joshi, R. Julian, D. Kalashnikov, Y. Kuang, I. Leal, K. Lee, S. Levine, Y. Lu, U. Malla, D. Manjunath, I. Mordatch, O. Nachum, C. Parada, J. Peralta, E. Perez, K. Pertsch, J. Quiambao, K. Rao, M. S. Ryoo, G. Salazar, P. R. Sanketi, K. Sayed, J. Singh, S. Sontakke, A. Stone, C. Tan, H. T. Tran, V. Vanhoucke, S. Vega, Q. Vuong, F. Xia, T. Xiao, P. Xu, S. Xu, T. Yu, and B. Zitkovich, “RT-1: robotics transformer for real-world control at scale,” in *Robotics: Science and Systems XIX, Daegu, Republic of Korea, July 10-14, 2023*, K. E. Bekris, K. Hauser, S. L. Herbert, and J. Yu, Eds., 2023. [Online]. Available: <https://doi.org/10.15607/RSS.2023.XIX.025>
- [8] Z. Mandi, F. Liu, K. Lee, and P. Abbeel, “Towards more generalizable one-shot visual imitation learning,” in *2022 International Conference on Robotics and Automation (ICRA)*. IEEE, 2022, pp. 2434–2444.
- [9] S. Stepputtis, J. Campbell, M. Phielipp, S. Lee, C. Baral, and H. Ben Amor, “Language-conditioned imitation learning for robot manipulation tasks,” *Advances in Neural Information Processing Systems*, vol. 33, pp. 13 139–13 150, 2020.
- [10] O. Mees, L. Hermann, E. Rosete-Beas, and W. Burgard, “Calvin: A benchmark for language-conditioned policy learning for long-horizon robot manipulation tasks,” *IEEE Robotics and Automation Letters (RA-L)*, vol. 7, no. 3, pp. 7327–7334, 2022.
- [11] M. Zare, P. M. Kebria, A. Khosravi, and S. Nahavandi, “A survey of imitation learning: Algorithms, recent developments, and challenges,” *IEEE Transactions on Cybernetics*, 2024.
- [12] S. James, M. Bloesch, and A. J. Davison, “Task-embedded control networks for few-shot imitation learning,” in *2nd Annual Conference on Robot Learning, CoRL 2018, Zürich, Switzerland*,

- 29-31 October 2018, *Proceedings*, ser. Proceedings of Machine Learning Research, vol. 87. PMLR, 2018, pp. 783–795. [Online]. Available: <http://proceedings.mlr.press/v87/james18a.html>
- [13] E. Jang, A. Irpan, M. Khansari, D. Kappler, F. Ebert, C. Lynch, S. Levine, and C. Finn, “Bc-z: Zero-shot task generalization with robotic imitation learning,” in *Conference on Robot Learning*. PMLR, 2022, pp. 991–1002.
 - [14] M. Shridhar, L. Manuelli, and D. Fox, “Perceiver-actor: A multi-task transformer for robotic manipulation,” in *Conference on Robot Learning*. PMLR, 2023, pp. 785–799.
 - [15] B. Fang, S. Jia, D. Guo, M. Xu, S. Wen, and F. Sun, “Survey of imitation learning for robotic manipulation,” *International Journal of Intelligent Robotics and Applications*, vol. 3, no. 4, pp. 362–369, 2019.
 - [16] O. Kroemer, S. Niekum, and G. Konidaris, “A review of robot learning for manipulation: Challenges, representations, and algorithms,” *The Journal of Machine Learning Research*, vol. 22, no. 1, pp. 1395–1476, 2021.
 - [17] E. Johns, “Coarse-to-fine imitation learning: Robot manipulation from a single demonstration,” in *2021 IEEE International Conference on Robotics and Automation (ICRA)*. IEEE, 2021, pp. 4613–4619.
 - [18] R. Caccavale, M. Saveriano, A. Finzi, and D. Lee, “Kinesthetic teaching and attentional supervision of structured tasks in human–robot interaction,” *Autonomous Robots*, vol. 43, no. 6, pp. 1291–1307, 2019.
 - [19] A. Mandlekar, Y. Zhu, A. Garg, J. Booher, M. Spero, A. Tung, J. Gao, J. Emmons, A. Gupta, E. Orbay *et al.*, “Roboturk: A crowdsourcing platform for robotic skill learning through imitation,” in *Conference on Robot Learning*. PMLR, 2018, pp. 879–893.

- [20] F. Ebert, Y. Yang, K. Schmeckpeper, B. Bucher, G. Georgakis, K. Daniilidis, C. Finn, and S. Levine, “Bridge Data: Boosting Generalization of Robotic Skills with Cross-Domain Datasets,” in *Proceedings of Robotics: Science and Systems*, New York City, NY, USA, June 2022.
- [21] A. Mandlekar, S. Nasiriany, B. Wen, I. Akinola, Y. Narang, L. Fan, Y. Zhu, and D. Fox, “Mimicgen: A data generation system for scalable robot learning using human demonstrations,” in *Conference on Robot Learning*. PMLR, 2023, pp. 1820–1864.
- [22] S. Dasari, F. Ebert, S. Tian, S. Nair, B. Bucher, K. Schmeckpeper, S. Singh, S. Levine, and C. Finn, “Robonet: Large-scale multi-robot learning,” in *Conference on Robot Learning*. PMLR, 2020, pp. 885–897.
- [23] M. Chang and S. Gupta, “One-shot visual imitation via attributed waypoints and demonstration augmentation,” in *2023 IEEE International Conference on Robotics and Automation (ICRA)*. IEEE, 2023, pp. 5055–5062.
- [24] D. Lee and C. Ott, “Incremental kinesthetic teaching of motion primitives using the motion refinement tube,” *Autonomous Robots*, vol. 31, pp. 115–131, 2011.
- [25] M. Saveriano, S.-i. An, and D. Lee, “Incremental kinesthetic teaching of end-effector and null-space motion primitives,” in *2015 IEEE International Conference on Robotics and Automation (ICRA)*. IEEE, 2015, pp. 3570–3575.
- [26] A. Mandlekar, J. Booher, M. Spero, A. Tung, A. Gupta, Y. Zhu, A. Garg, S. Savarese, and L. Fei-Fei, “Scaling robot supervision to hundreds of hours with roboturk: Robotic manipulation dataset through human reasoning and dexterity,” in *2019 IEEE/RSJ International Conference on Intelligent Robots and Systems (IROS)*. IEEE, 2019, pp. 1048–1055.

- [27] C. Systems, “Cyberforce.” [Online]. Available: <http://www.cyberglovesystems.com/cyberforce>
- [28] D. Systems, “Touch.” [Online]. Available: <https://it.3dsystems.com/haptics-devices/touch>
- [29] Y. Zhu, J. Wong, A. Mandlekar, R. Martín-Martín, A. Joshi, S. Nasiriany, and Y. Zhu, “robosuite: A modular simulation framework and benchmark for robot learning,” *arXiv preprint arXiv:2009.12293*, 2020.
- [30] H. Liu, C. Zhang, Y. Zhu, C. Jiang, and S.-C. Zhu, “Mirroring without overimitation: Learning functionally equivalent manipulation actions,” *Proceedings of the AAAI Conference on Artificial Intelligence*, vol. 33, no. 01, pp. 8025–8033, Jul. 2019.
- [31] L. Smith, N. Dhawan, M. Zhang, P. Abbeel, and S. Levine, “AVID: Learning Multi-Stage Tasks via Pixel-Level Translation of Human Videos,” in *Proceedings of Robotics: Science and Systems*, Corvalis, Oregon, USA, July 2020.
- [32] S. Nakaoaka, A. Nakazawa, F. Kanehiro, K. Kaneko, M. Morisawa, H. Hirukawa, and K. Ikeuchi, “Learning from observation paradigm: Leg task models for enabling a biped humanoid robot to imitate human dances,” *The International Journal of Robotics Research*, vol. 26, no. 8, pp. 829–844, 2007.
- [33] H. Liu, X. Xie, M. Millar, M. Edmonds, F. Gao, Y. Zhu, V. J. Santos, B. Rothrock, and S.-C. Zhu, “A glove-based system for studying hand-object manipulation via joint pose and force sensing,” in *2017 IEEE/RSJ International Conference on Intelligent Robots and Systems (IROS)*. IEEE, 2017, pp. 6617–6624.
- [34] F. Torabi, G. Warnell, and P. Stone, “Recent advances in imitation learning from observation,” in *Proceedings of the Twenty-Eighth International Joint Conference on Artificial Intelligence*,

- IJCAI-19.* International Joint Conferences on Artificial Intelligence Organization, 7 2019, pp. 6325–6331. [Online]. Available: <https://doi.org/10.24963/ijcai.2019/882>
- [35] H. Xiong, Q. Li, Y.-C. Chen, H. Bharadhwaj, S. Sinha, and A. Garg, “Learning by watching: Physical imitation of manipulation skills from human videos,” in *2021 IEEE/RSJ International Conference on Intelligent Robots and Systems (IROS)*. IEEE, 2021, pp. 7827–7834.
 - [36] C. Wang, L. Fan, J. Sun, R. Zhang, L. Fei-Fei, D. Xu, Y. Zhu, and A. Anandkumar, “Mimicplay: Long-horizon imitation learning by watching human play,” in *Conference on Robot Learning*. PMLR, 2023, pp. 201–221.
 - [37] Z. Qian, M. You, H. Zhou, X. Xu, H. Fu, J. Xue, and B. He, *IEEE Transactions on Automation Science and Engineering*, 2024.
 - [38] L. P. Kaelbling, M. L. Littman, and A. W. Moore, “Reinforcement learning: A survey,” *Journal of artificial intelligence research*, vol. 4, pp. 237–285, 1996.
 - [39] B. D. Argall, S. Chernova, M. Veloso, and B. Browning, “A survey of robot learning from demonstration,” *Robotics and autonomous systems*, vol. 57, no. 5, pp. 469–483, 2009.
 - [40] A. Hussein, M. M. Gaber, E. Elyan, and C. Jayne, “Imitation learning: A survey of learning methods,” *ACM Computing Surveys (CSUR)*, vol. 50, no. 2, pp. 1–35, 2017.
 - [41] B. Zheng, S. Verma, J. Zhou, I. Tsang, and F. Chen, “Imitation learning: Progress, taxonomies and opportunities,” *arXiv preprint arXiv:2106.12177*, 2021.
 - [42] D. A. Pomerleau, “Alvinn: An autonomous land vehicle in a neural network,” *Advances in neural information processing systems*, vol. 1, 1988.

- [43] A. Ijspeert, J. Nakanishi, and S. Schaal, “Learning attractor landscapes for learning motor primitives,” *Advances in neural information processing systems*, vol. 15, 2002.
- [44] A. J. Ijspeert, J. Nakanishi, H. Hoffmann, P. Pastor, and S. Schaal, “Dynamical movement primitives: learning attractor models for motor behaviors,” *Neural computation*, vol. 25, no. 2, pp. 328–373, 2013.
- [45] W. Si, N. Wang, and C. Yang, “Composite dynamic movement primitives based on neural networks for human–robot skill transfer,” *Neural Computing and Applications*, vol. 35, no. 32, pp. 23 283–23 293, 2023.
- [46] J. Li, J. Wang, S. Wang, and C. Yang, “Human–robot skill transmission for mobile robot via learning by demonstration,” *Neural Computing and Applications*, vol. 35, no. 32, pp. 23 441–23 451, 2023.
- [47] Y. Fanger, J. Umlauft, and S. Hirche, “Gaussian processes for dynamic movement primitives with application in knowledge-based cooperation,” in *2016 IEEE/RSJ International Conference on Intelligent Robots and Systems (IROS)*. IEEE, 2016, pp. 3913–3919.
- [48] A. Paraschos, C. Daniel, J. R. Peters, and G. Neumann, “Probabilistic movement primitives,” *Advances in neural information processing systems*, vol. 26, 2013.
- [49] M. Saveriano, F. J. Abu-Dakka, A. Kramberger, and L. Peternel, “Dynamic movement primitives in robotics: A tutorial survey,” *The International Journal of Robotics Research*, vol. 42, no. 13, pp. 1133–1184, 2023.
- [50] Y. Zhou, J. Gao, and T. Asfour, “Learning via-point movement primitives with inter-and extrapolation capabilities,” in *2019 IEEE/RSJ International Conference on Intelligent Robots and Systems (IROS)*. IEEE, 2019, pp. 4301–4308.

-
- [51] F. Meier, E. Theodorou, F. Stulp, and S. Schaal, “Movement segmentation using a primitive library,” in *2011 IEEE/RSJ International Conference on Intelligent Robots and Systems*. IEEE, 2011, pp. 3407–3412.
 - [52] A. Agostini, M. Saveriano, D. Lee, and J. Piater, “Manipulation planning using object-centered predicates and hierarchical decomposition of contextual actions,” *IEEE Robotics and Automation Letters*, vol. 5, no. 4, pp. 5629–5636, 2020.
 - [53] S. Ross and D. Bagnell, “Efficient reductions for imitation learning,” in *Proceedings of the thirteenth international conference on artificial intelligence and statistics*. JMLR Workshop and Conference Proceedings, 2010, pp. 661–668.
 - [54] S. Ross, G. Gordon, and D. Bagnell, “A reduction of imitation learning and structured prediction to no-regret online learning,” in *Proceedings of the fourteenth international conference on artificial intelligence and statistics*. JMLR Workshop and Conference Proceedings, 2011, pp. 627–635.
 - [55] M. Laskey, C. Chuck, J. Lee, J. Mahler, S. Krishnan, K. Jamieson, A. Dragan, and K. Goldberg, “Comparing human-centric and robot-centric sampling for robot deep learning from demonstrations,” in *2017 IEEE International Conference on Robotics and Automation (ICRA)*. IEEE, 2017, pp. 358–365.
 - [56] M. Kelly, C. Sidrane, K. Driggs-Campbell, and M. J. Kochenderfer, “Hg-dagger: Interactive imitation learning with human experts,” in *2019 International Conference on Robotics and Automation (ICRA)*. IEEE, 2019, pp. 8077–8083.
 - [57] A. Mandlekar, D. Xu, R. Martín-Martín, Y. Zhu, L. Fei-Fei, and S. Savarese, “Human-in-the-loop imitation learning using remote tele-operation,” *arXiv preprint arXiv:2012.06733*, 2020.

- [58] E. Chisari, T. Welschehold, J. Boedecker, W. Burgard, and A. Valada, “Correct me if i am wrong: Interactive learning for robotic manipulation,” *IEEE Robotics and Automation Letters*, vol. 7, no. 2, pp. 3695–3702, 2022.
- [59] V. Bhutani, A. Majumder, M. Vankadari, S. Dutta, A. Asati, and S. Kumar, “Attentive one-shot meta-imitation learning from visual demonstration,” in *2022 International Conference on Robotics and Automation (ICRA)*, 2022, pp. 8584–8590.
- [60] B. Ichter, A. Brohan, Y. Chebotar, C. Finn, K. Hausman, A. Herzog, D. Ho, J. Ibarz, A. Irpan, E. Jang, R. Julian, D. Kalashnikov, S. Levine, Y. Lu, C. Parada, K. Rao, P. Sermanet, A. Toshev, V. Vanhoucke, F. Xia, T. Xiao, P. Xu, M. Yan, N. Brown, M. Ahn, O. Cortes, N. Sievers, C. Tan, S. Xu, D. Reyes, J. Rettinghouse, J. Quiambao, P. Pastor, L. Luu, K. Lee, Y. Kuang, S. Jesmonth, N. J. Joshi, K. Jeffrey, R. J. Ruano, J. Hsu, K. Gopalakrishnan, B. David, A. Zeng, and C. K. Fu, “Do as I can, not as I say: Grounding language in robotic affordances,” in *Conference on Robot Learning, CoRL 2022, 14-18 December 2022, Auckland, New Zealand*, ser. Proceedings of Machine Learning Research, K. Liu, D. Kulic, and J. Ichnowski, Eds., vol. 205. PMLR, 2022, pp. 287–318. [Online]. Available: <https://proceedings.mlr.press/v205/ichter23a.html>
- [61] O. Mees, L. Hermann, and W. Burgard, “What matters in language conditioned robotic imitation learning over unstructured data,” *IEEE Robotics and Automation Letters (RA-L)*, vol. 7, no. 4, pp. 11205–11212, 2022.
- [62] Y. Jiang, A. Gupta, Z. Zhang, G. Wang, Y. Dou, Y. Chen, L. Fei-Fei, A. Anandkumar, Y. Zhu, and L. Fan, “Vima: General robot manipulation with multimodal prompts,” in *Fortieth International Conference on Machine Learning*, 2023.
- [63] C. Finn, P. Abbeel, and S. Levine, “Model-agnostic meta-learning

- for fast adaptation of deep networks,” in *International conference on machine learning*. PMLR, 2017, pp. 1126–1135.
- [64] C. Finn, T. Yu, T. Zhang, P. Abbeel, and S. Levine, “One-shot visual imitation learning via meta-learning,” in *Conference on robot learning*. PMLR, 2017, pp. 357–368.
 - [65] T. Yu, C. Finn, S. Dasari, A. Xie, T. Zhang, P. Abbeel, and S. Levine, “One-shot imitation from observing humans via domain-adaptive meta-learning,” in *Proceedings of Robotics: Science and Systems*, Pittsburgh, Pennsylvania, June 2018.
 - [66] T. Yu, P. Abbeel, S. Levine, and C. Finn, “One-shot hierarchical imitation learning of compound visuomotor tasks,” *arXiv preprint arXiv:1810.11043*, 2018.
 - [67] Y. Duan, M. Andrychowicz, B. Stadie, O. Jonathan Ho, J. Schneider, I. Sutskever, P. Abbeel, and W. Zaremba, “One-shot imitation learning,” *Advances in neural information processing systems*, vol. 30, 2017.
 - [68] R. Girshick, “Fast r-cnn,” in *2015 IEEE International Conference on Computer Vision (ICCV)*, 2015, pp. 1440–1448.
 - [69] J. Pennington, R. Socher, and C. D. Manning, “Glove: Global vectors for word representation,” in *Proceedings of the 2014 conference on empirical methods in natural language processing (EMNLP)*, 2014, pp. 1532–1543.
 - [70] E. Perez, F. Strub, H. De Vries, V. Dumoulin, and A. Courville, “Film: Visual reasoning with a general conditioning layer,” in *Proceedings of the AAAI conference on artificial intelligence*, vol. 32, 2018.
 - [71] M. Tan and Q. Le, “Efficientnet: Rethinking model scaling for convolutional neural networks,” in *International conference on machine learning*. PMLR, 2019, pp. 6105–6114.

- [72] D. Cer, Y. Yang, S.-y. Kong, N. Hua, N. Limtiaco, R. S. John, N. Constant, M. Guajardo-Cespedes, S. Yuan, C. Tar *et al.*, “Universal sentence encoder,” *arXiv preprint arXiv:1803.11175*, 2018.
- [73] M. Ryoo, A. Piergiovanni, A. Arnab, M. Dehghani, and A. Angelova, “Tokenlearner: Adaptive space-time tokenization for videos,” *Advances in neural information processing systems*, vol. 34, pp. 12 786–12 797, 2021.
- [74] K. Grill-Spector, “The neural basis of object perception,” *Current opinion in neurobiology*, vol. 13, no. 2, pp. 159–166, 2003.
- [75] O. Mees, J. Borja-Diaz, and W. Burgard, “Grounding language with visual affordances over unstructured data,” in *2023 IEEE International Conference on Robotics and Automation (ICRA)*. IEEE, 2023, pp. 11 576–11 582.
- [76] M. Reuss, Ö. E. Yağmurlu, F. Wenzel, and R. Lioutikov, “Multimodal diffusion transformer: Learning versatile behavior from multimodal goals,” in *First Workshop on Vision-Language Models for Navigation and Manipulation at ICRA 2024*, 2024.
- [77] M. Shridhar, L. Manuelli, and D. Fox, “Cliport: What and where pathways for robotic manipulation,” in *Conference on robot learning*. PMLR, 2022, pp. 894–906.
- [78] A. Radford, J. W. Kim, C. Hallacy, A. Ramesh, G. Goh, S. Agarwal, G. Sastry, A. Askell, P. Mishkin, J. Clark *et al.*, “Learning transferable visual models from natural language supervision,” in *International conference on machine learning*. PMLR, 2021, pp. 8748–8763.
- [79] A. Zeng, P. Florence, J. Tompson, S. Welker, J. Chien, M. Attarian, T. Armstrong, I. Krasin, D. Duong, V. Sindhwani *et al.*, “Transporter networks: Rearranging the visual world for robotic manipulation,” in *Conference on Robot Learning*. PMLR, 2021, pp. 726–747.

- [80] K. He, X. Zhang, S. Ren, and J. Sun, “Deep residual learning for image recognition,” in *2016 IEEE Conference on Computer Vision and Pattern Recognition (CVPR)*, 2016, pp. 770–778.
- [81] A. Vaswani, N. Shazeer, N. Parmar, J. Uszkoreit, L. Jones, A. N. Gomez, L. u. Kaiser, and I. Polosukhin, “Attention is all you need,” in *Advances in Neural Information Processing Systems*, I. Guyon, U. V. Luxburg, S. Bengio, H. Wallach, R. Fergus, S. Vishwanathan, and R. Garnett, Eds., vol. 30. Curran Associates, Inc., 2017.
- [82] Z. J. Cui, Y. Wang, N. M. M. Shafiullah, and L. Pinto, “From play to policy: Conditional behavior generation from uncurated robot data,” in *The Eleventh International Conference on Learning Representations*, 2023.
- [83] C. Devin, P. Abbeel, T. Darrell, and S. Levine, “Deep object-centric representations for generalizable robot learning,” in *2018 IEEE International Conference on Robotics and Automation (ICRA)*. IEEE, 2018, pp. 7111–7118.
- [84] J. Park, Y. Seo, C. Liu, L. Zhao, T. Qin, J. Shin, and T.-Y. Liu, “Object-aware regularization for addressing causal confusion in imitation learning,” *Advances in Neural Information Processing Systems*, vol. 34, pp. 3029–3042, 2021.
- [85] S. Belkhale and D. Sadigh, “Plato: Predicting latent affordances through object-centric play,” in *Conference on Robot Learning*. PMLR, 2023, pp. 1424–1434.
- [86] Y. Zhu, A. Joshi, P. Stone, and Y. Zhu, “Viola: Imitation learning for vision-based manipulation with object proposal priors,” in *Conference on Robot Learning*. PMLR, 2023, pp. 1199–1210.
- [87] Y. Zhu, Z. Jiang, P. Stone, and Y. Zhu, “Learning generalizable manipulation policies with object-centric 3d representations,” in *Conference on Robot Learning*. PMLR, 2023, pp. 3418–3433.

- [88] T.-Y. Lin, M. Maire, S. Belongie, J. Hays, P. Perona, D. Ramanan, P. Dollár, and C. L. Zitnick, “Microsoft coco: Common objects in context,” in *Computer Vision–ECCV 2014: 13th European Conference, Zurich, Switzerland, September 6–12, 2014, Proceedings, Part V 13*. Springer, 2014, pp. 740–755.
- [89] D. Kalashnikov, A. Irpan, P. Pastor, J. Ibarz, A. Herzog, E. Jang, D. Quillen, E. Holly, M. Kalakrishnan, V. Vanhoucke *et al.*, “Scalable deep reinforcement learning for vision-based robotic manipulation,” in *Conference on robot learning*. PMLR, 2018, pp. 651–673.
- [90] P. Abbeel and A. Y. Ng, “Apprenticeship learning via inverse reinforcement learning,” in *Proceedings of the twenty-first international conference on Machine learning*, 2004, p. 1.
- [91] N. D. Ratliff, J. A. Bagnell, and M. A. Zinkevich, “Maximum margin planning,” in *Proceedings of the 23rd international conference on Machine learning*, 2006, pp. 729–736.
- [92] N. D. Ratliff, D. Silver, and J. A. Bagnell, “Learning to search: Functional gradient techniques for imitation learning,” *Autonomous Robots*, vol. 27, no. 1, pp. 25–53, 2009.
- [93] B. D. Ziebart, A. L. Maas, J. A. Bagnell, A. K. Dey *et al.*, “Maximum entropy inverse reinforcement learning.” in *Aaai*, vol. 8. Chicago, IL, USA, 2008, pp. 1433–1438.
- [94] M. Wulfmeier, P. Ondruska, and I. Posner, “Maximum entropy deep inverse reinforcement learning,” *arXiv preprint arXiv:1507.04888*, 2015.
- [95] C. Finn, S. Levine, and P. Abbeel, “Guided cost learning: Deep inverse optimal control via policy optimization,” in *International conference on machine learning*. PMLR, 2016, pp. 49–58.

- [96] S. Levine and P. Abbeel, “Learning neural network policies with guided policy search under unknown dynamics,” *Advances in neural information processing systems*, vol. 27, 2014.
- [97] N. Das, S. Bechtle, T. Davchev, D. Jayaraman, A. Rai, and F. Meier, “Model-based inverse reinforcement learning from visual demonstrations,” in *Conference on Robot Learning*. PMLR, 2021, pp. 1930–1942.
- [98] J. Ho and S. Ermon, “Generative adversarial imitation learning,” *Advances in neural information processing systems*, vol. 29, 2016.
- [99] J. Schulman, S. Levine, P. Abbeel, M. Jordan, and P. Moritz, “Trust region policy optimization,” in *International conference on machine learning*. PMLR, 2015, pp. 1889–1897.
- [100] J. Ho, J. Gupta, and S. Ermon, “Model-free imitation learning with policy optimization,” in *International conference on machine learning*. PMLR, 2016, pp. 2760–2769.
- [101] G. Brockman, V. Cheung, L. Pettersson, J. Schneider, J. Schulman, J. Tang, and W. Zaremba, “Openai gym,” *arXiv preprint arXiv:1606.01540*, 2016.
- [102] I. Kostrikov, K. K. Agrawal, D. Dwibedi, S. Levine, and J. Tompson, “Discriminator-actor-critic: Addressing sample inefficiency and reward bias in adversarial imitation learning,” in *International Conference on Learning Representations*, 2018.
- [103] J. Fu, K. Luo, and S. Levine, “Learning robust rewards with adversarial inverse reinforcement learning,” in *International Conference on Learning Representations*, 2018.
- [104] S. K. S. Ghasemipour, R. Zemel, and S. Gu, “A divergence minimization perspective on imitation learning methods,” in *Conference on Robot Learning*. PMLR, 2020, pp. 1259–1277.

- [105] Y. Liu, A. Gupta, P. Abbeel, and S. Levine, “Imitation from observation: Learning to imitate behaviors from raw video via context translation,” in *2018 IEEE International Conference on Robotics and Automation (ICRA)*. IEEE, 2018, pp. 1118–1125.
- [106] S. Reddy, A. D. Dragan, and S. Levine, “Sql: Imitation learning via reinforcement learning with sparse rewards,” in *International Conference on Learning Representations*, 2019.
- [107] K. Zolna, S. Reed, A. Novikov, S. G. Colmenarejo, D. Budden, S. Cabi, M. Denil, N. de Freitas, and Z. Wang, “Task-relevant adversarial imitation learning,” in *Conference on Robot Learning*. PMLR, 2021, pp. 247–263.
- [108] R. Rafailov, T. Yu, A. Rajeswaran, and C. Finn, “Visual adversarial imitation learning using variational models,” *Advances in Neural Information Processing Systems*, vol. 34, pp. 3016–3028, 2021.
- [109] G. Barth-Maron, M. W. Hoffman, D. Budden, W. Dabney, D. Horgan, D. Tb, A. Muldal, N. Heess, and T. Lillicrap, “Distributed distributional deterministic policy gradients,” *arXiv preprint arXiv:1804.08617*, 2018.
- [110] J. Li, T. Lu, X. Cao, Y. Cai, and S. Wang, “Meta-imitation learning by watching video demonstrations,” in *International Conference on Learning Representations*, 2021.
- [111] J.-Y. Zhu, T. Park, P. Isola, and A. A. Efros, “Unpaired image-to-image translation using cycle-consistent adversarial networks,” in *Proceedings of the IEEE international conference on computer vision*, 2017, pp. 2223–2232.
- [112] P. Sermanet, C. Lynch, Y. Chebotar, J. Hsu, E. Jang, S. Schaal, S. Levine, and G. Brain, “Time-contrastive networks: Self-supervised learning from video,” in *2018 IEEE international conference on robotics and automation (ICRA)*. IEEE, 2018, pp. 1134–1141.

-
- [113] F. Schroff, D. Kalenichenko, and J. Philbin, “Facenet: A unified embedding for face recognition and clustering,” in *Proceedings of the IEEE conference on computer vision and pattern recognition*, 2015, pp. 815–823.
 - [114] K. Zakka, A. Zeng, P. Florence, J. Tompson, J. Bohg, and D. Dwibedi, “Xirl: Cross-embodiment inverse reinforcement learning,” in *Conference on Robot Learning*. PMLR, 2022, pp. 537–546.
 - [115] J. Merel, Y. Tassa, D. TB, S. Srinivasan, J. Lemmon, Z. Wang, G. Wayne, and N. Heess, “Learning human behaviors from motion capture by adversarial imitation,” *arXiv preprint arXiv:1707.02201*, 2017.
 - [116] F. Torabi, G. Warnell, and P. Stone, “Generative adversarial imitation from observation,” *arXiv preprint arXiv:1807.06158*, 2018.
 - [117] ——, “Behavioral cloning from observation,” in *Proceedings of the 27th International Joint Conference on Artificial Intelligence*, 2018, pp. 4950–4957.
 - [118] ——, “Dealio: Data-efficient adversarial learning for imitation from observation,” in *2021 IEEE/RSJ International Conference on Intelligent Robots and Systems (IROS)*. IEEE, 2021, pp. 2391–2397.
 - [119] Y. Chebotar, K. Hausman, M. Zhang, G. Sukhatme, S. Schaal, and S. Levine, “Combining model-based and model-free updates for trajectory-centric reinforcement learning,” in *International conference on machine learning*. PMLR, 2017, pp. 703–711.
 - [120] A. Nair, D. Chen, P. Agrawal, P. Isola, P. Abbeel, J. Malik, and S. Levine, “Combining self-supervised learning and imitation for vision-based rope manipulation,” in *2017 IEEE international conference on robotics and automation (ICRA)*. IEEE, 2017, pp. 2146–2153.

- [121] X. Guo, S. Chang, M. Yu, G. Tesauro, and M. Campbell, “Hybrid reinforcement learning with expert state sequences,” in *Proceedings of the AAAI Conference on Artificial Intelligence*, vol. 33, 2019, pp. 3739–3746.
- [122] I. Radosavovic, X. Wang, L. Pinto, and J. Malik, “State-only imitation learning for dexterous manipulation,” in *2021 IEEE/RSJ International Conference on Intelligent Robots and Systems (IROS)*. IEEE, 2021, pp. 7865–7871.
- [123] V. Mnih, A. P. Badia, M. Mirza, A. Graves, T. Lillicrap, T. Harley, D. Silver, and K. Kavukcuoglu, “Asynchronous methods for deep reinforcement learning,” in *International conference on machine learning*. PMLR, 2016, pp. 1928–1937.
- [124] A. Rajeswaran, V. Kumar, A. Gupta, G. Vezzani, J. Schulman, E. Todorov, and S. Levine, “Learning complex dexterous manipulation with deep reinforcement learning and demonstrations,” in *Proceedings of Robotics: Science and Systems*, Pittsburgh, Pennsylvania, June 2018.
- [125] M. Zhang, S. Vikram, L. Smith, P. Abbeel, M. Johnson, and S. Levine, “Solar: Deep structured representations for model-based reinforcement learning,” in *International Conference on Machine Learning*. PMLR, 2019, pp. 7444–7453.
- [126] D. P. Kingma and M. Welling, “Auto-Encoding Variational Bayes,” in *2nd International Conference on Learning Representations, ICLR 2014, Banff, AB, Canada, April 14-16, 2014, Conference Track Proceedings*, 2014.

List of Figures

1.1	Examples of direct demonstration	7
1.2	Examples of indirect demonstration	10
1.3	Taxonomy of LfD methods, divided based on type of demonstration and the learning algorithm used to learn the learner policy π^L	12
1.4	Graphical representation of the idea behind VMP [50]. The final trajectory y is represented as the sum of two components: the elementary trajectory h , and the shape modulation f . The elementary trajectory can directly connect two points (e.g., start and goal points) with a linear segment.	18
1.5	Architecture proposed in [4]	21
1.6	Multi-Task Imitation Learning Taxonomy	25
1.7	Diagram of MAML algorithm, which optimizes for a representation θ that can quickly adapt to new tasks	28
1.8	Tasks performed in [65]. (Top row) Human demonstration, (Bottom row) robot demonstration. (Left) Placing task, (Middle) pushing task, (Right) pick-and-place task.	30
1.9	The Temporal Adaptation Loss architecture applies 1D temporal convolutional layers to the stacked embeddings generated by the policy π from the frames of the human video demonstration.	30

1.10	Architecture proposed in [9]. The <i>Semantic Model</i> takes in input the image I and the command v , generating a command conditioned embedding e . The <i>Control Module</i> receives in input the embedding e and the current robot state r_t and produces the next control signal.	33
1.11	(Left) Set of object used in [9]. (Right) Sample of task execution (right)	33
1.12	Architecture proposed in [13]. Here, the Task Embedding is injected directly in the Feature Maps generated by the ResNet-18.	34
1.13	Examples of household scenarios in RT-1 large-scale dataset.	35
1.14	RT-1 Language-Conditioned Transformer based architecture proposed in [7].	36
1.15	Environment proposed in CALVIN benchmark [?]. The environments have different textures and all static elements such as the sliding door, the drawer, the light button, and switch are positioned differently	38
1.16	The Multimodal Diffusion Transformer (MDT) architecture proposed in [76]	39
1.17	The Dual Stream architecture proposed in [77] consists of two parallel streams: a semantic stream and a spatial stream. The semantic stream utilizes a frozen CLIP ResNet50 to encode the RGB input, with the decoder layers conditioned by tiled language features from the CLIP sentence encoder. Meanwhile, the spatial stream encodes the RGB-D input, and its decoder layers are laterally fused with those of the semantic stream. The final output is a map of dense pixel-wise features, which is used to predict pick or place affordances.	41
1.18	Example of affordance map. (Left) The top-view input image. (Center) The affordance map for the pick-operation, since the task is to grab cherries the map highlights the two pickable cherries. (Right) The affordance map for the place operation.	42

1.19	Architecture proposed in [12]. The <i>Task Embedding Net</i> generates the embedding representing the task to be performed given the goal image. The <i>Control Net</i> implements the policy, and takes in input the current observation and the tiled task embedding	43
1.20	Transformer based architecture proposed in [6]. The Transformer network is used to create task-specific representation, given context and observation features computed with ResNet-18.	45
1.21	Validation setting proposed in [6]. The 16 tasks consist of taking an object (a-b) to a bin (1-4). On the left there is the demonstrator robot, while on the right there is the agent robot.	46
1.22	(Left) The TOSIL architecture, as proposed in [6]. (Right) The MOSAIC architecture, as introduced in [8]. In the MO-SAIC architecture, the original encoder-decoder Transformer architecture has been replaced with an encoder-only architecture featuring self-attention modules.	47
1.23	The evaluation tasks proposed in [8] consist of a total of 7 tasks with 61 semantic variations.	48
1.24	AWDA framework proposed in [23]. The task inference network $f(v, o)$ predicts a sequence of attributed waypoints (red dots) that are achieved by hand-defined motion primitives. The original data are augmented with free-space motion trajectories and asymmetric demonstration mixup in order to reduce the correlation between tasks and task content. . . .	51

1.25	Robotic vision framework proposed in [83]. The framework is divided into different stages: Meta-Attention : Generates object proposals from an input image, trained on an object detection dataset, and shared across tasks; Task-Specific Attention : Focuses on relevant objects for a task using the meta-attention’s semantic features; Soft Attention : Distributes attention as probabilities over object proposals using a Boltzmann distribution; Movement Prediction Network : Combines attended object information with the robot’s state to predict the next action.	55
1.26	Pouring task setting proposed in [83]. (Left) Mugs used for evaluation. Note that only the brown mug was seen during training. Center: Successful pouring into the pink mug. (Right) Pouring into the brown mug in a cluttered environment that was not seen during training.	56
1.27	The region proposals (meta-attention) are drawn in blue and the task-specific attended regions are drawn in red. For the Pouring task with distractor mug (pink) and target mug (brown), the attention locks on to the brown mug as its position defines the trajectory. For the sweeping task, two attention vectors are used, one attends to the orange and one attends to the dustpan.	57
1.28	VIOLA architecture proposed in [86].	58
1.29	Simulation tasks on which the VIOLA [86] method was tested. (Left) Sorting task. (Center) Stacking task. (Right) BUDS-Kitchen task	58

1.30 PLATO architecture proposed in [85]. The architecture is composed of different stages. (1) The posterior encoder E encodes the interaction sequence $\tau^{(i)}$ into the affordance z . (2) The prior encoder E' encodes the object initial state $o_1^{(i)}$ and goal state o_g to predict z , with o_g sampled after the interaction. (3) The policy is trained to output actions during the interaction period conditioned on the affordance. Simultaneously, (4) it is trained to output actions during the pre-interaction period conditioned on the “future” affordance.	60
1.31 Testing scenarios and primitives proposed in [85]. (Top) Block2D Environment primitive examples. (Center) Block3D and Block3DPlatform primitive examples. (Bottom) The left image shows an example primitive in Mug3D-Platforms . The right three images show sample tasks from Playroom3D .	61
1.32 Architecture proposed in [97]	66
1.33 The performance comparison proposed in [98] is presented here. The y-axis shows the scaled reward, where the expert’s reward is set to 1 and the random baseline is set to 0. The IRL baselines FEM and GTAL refer to the IRL algorithm described in [100], but with different cost functions.	70
1.34 Tasks solved in [107]	72
1.35 Experimental results on tasks without and with spurious features [107]	73
1.36 Representation of embodiment mismatch problem . (Left) The source domain represented by a video of human performing a task. (Right) The target domain, represented by the robot that executes the observed task	75
1.37 Examples of how the mismatch between demonstrator viewpoint and learner viewpoint can be handled.	78
1.38 Learning from Observation taxonomy	79
1.39 Architecture proposed by [35]	81
1.40 Experimental results reported in [116]	83

1.41 Representation of the learning procedure proposed by [117]	85
1.42 DEAILO: (1.42a) Control Tasks, (1.42b) Performance Level	87

List of Tables

1.1	Statistics of Training set, and Test Success rate [4]	21
1.2	Distribution of tasks in large-scale dataset proposed in [7] .	36
1.3	Results reported in [7] by training the same model RT-1 with different dataset size	37
1.4	Results obtained in single-task and multi-task one-shot imitation learning [8].	49
1.5	Success rates achieved using the MOSAIC and AWDA methods. In this scenario, training is conducted on 5 out of the 6 tasks, with the remaining task reserved for testing.	52
1.6	Observation and Action space for the tasks used in [98] . .	71